



Updated System of SI Levels Using Fourier Transform Infrared Spectroscopy in the Range from 800 to 11,000 cm⁻¹

S. Civiš¹ , A. Kramida² , E. M. Zanozina¹ , J. Kubišta¹ , P. Kubelík¹ , M. Ferus¹ , and V. E. Chernov³
¹ J. Heyrovský Institute of Physical Chemistry, Academy of Sciences of the Czech Republic, Dolejškova 3, 18223 Prague 8, Czech Republic; civis@jh-inst.cas.cz
² National Institute of Standards and Technology, Gaithersburg, MD 20899, USA
³ Voronezh State University, 394018 Voronezh, Russia

Received 2023 June 6; revised 2024 July 8; accepted 2024 July 10; published 2024 September 24

Abstract

In this study we report on high-precision laboratory measurements of transition wavenumbers for 172 atomic sulfur lines in the infrared region 800–11,000 cm⁻¹ using Fourier transform spectroscopy techniques. Our analysis includes 96 lines that have not been previously measured in the laboratory. We also correct several sulfur energy-level measurements reported in earlier studies. These refined measurements are important for a range of scientific disciplines, such as astrophysics, atmospheric chemistry, and combustion plasma physics. We have used the combined list of all observed lines to derive a refined set of sulfur energy levels. For about half of all nonautoionizing levels, the uncertainties have been reduced by a factor between 2 and 23. From the newly measured nonpenetrating (high-*l*) Rydberg levels we have also obtained the first ionization energy of the S atom, IE = 83,559.170(11) cm⁻¹, which is more accurate than the currently recommended value by 2 orders of magnitude. Our analysis has led to a significantly more accurate result than the earlier set of Ritz wavelengths with observed intensities reduced to a common uniform scale and an extended list of recommended transition probabilities.

Unified Astronomy Thesaurus concepts: [Atomic data \(2216\)](#); [Atomic spectroscopy \(2099\)](#); [High resolution spectroscopy \(2096\)](#); [Infrared spectroscopy \(2285\)](#)

Materials only available in the online version of record: machine-readable tables

1. Introduction

Studies of atomic spectra play a crucial role in understanding the fundamental principles of atomic physics and chemistry. Sulfur as a key element has been a subject of great interest among researchers due to its vital role in various chemical, biological, and environmental processes (Walsh 2020). Sulfur is one of the most abundant elements in the Universe (next after H, C, N, and O in the solar system). Sulfur abundance and distribution provide important information about the chemical evolution of galaxies, stars, and planets. For instance, as a compositional tracer, sulfur helps us to understand the links between planetary composition and formation processes in protoplanetary disks (Kama et al. 2019; Turrini et al. 2021). Sulfur is used in abundance studies of planetary nebulae targeting chemical evolution at particular locations in the Galaxy (Kwitter & Henry 2001; Milingo et al. 2002; Bernard-Salas et al. 2008). Including sulfur into thermochemical calculations is important for modeling the atmospheric chemistry of giant planets, brown dwarfs, and extrasolar giant planets (Visscher et al. 2006).

Knowledge of the atomic sulfur spectrum with high precision is crucial in interpreting the data acquired by ground and space observatories. The instrumentation on board the Hubble Space Telescope has made it possible to resolve the neutral atomic sulfur (S I) lines near 1479 Å due to emission to the ground $3s^23p^4\ ^3P$ term from the $3s^23p^3(^2P^o)4s^3D^o$ (allowed) and the $3s^23p^3(^4S^o)3d^5D$ (intercombination) terms. These

emission lines, together with the lines near 1814 Å (allowed transitions from $3s^23p^3(^4S^o)4s^3S^o$) and 1900 Å (intercombination transitions from $3s^23p^3(^4S^o)4s^5S^o$), were investigated in the study of both optically thick and thin spectral lines emitted by Io's atmosphere (Feaga et al. 2002). The electric-dipole-forbidden (M1+E2) [S I] line at 25.249 μm ($3s^23p^4\ ^3P_1-^3P_2$ fine-structure transition) observed by the Spitzer Infrared Spectrograph was studied to clarify the problem of “missing sulfur” in the interstellar medium (Anderson et al. 2013).

Numerous sulfur lines (more than 80) have been observed in the spectra of the Sun, as well as other astrophysical objects. Well-known S I emission lines at 1814 Å, 1479 Å, and 1429 Å have been observed in the International Ultraviolet Explorer Spectra in the vicinity of Io (Ballester et al. 1987), in the Hopkins Ultraviolet Telescope spectra of the Io plasma torus (Durrance et al. 1983) and in the far-ultraviolet spectra of α-Orionis by the Goddard High Resolution Spectrograph on board the Hubble Space Telescope (Carpenter et al. 1994).

Federman & Cardelli (1995) analyzed sulfur absorption in interstellar gas toward ζ-Ophiuchi in order to obtain a set of self-consistent absorption oscillator strengths (*f*-values) for approximately 20 S I lines. This analysis was possible because precisely determined experimental oscillator strengths are available for several S I multiplets (Doering 1990; Beideck et al. 1994), from which the column density and Doppler parameter were derived. Doering (1990) measured relative oscillator strengths for the multiplets at 1814 Å, 1479 Å, and 1429 Å using the method of electron energy loss spectroscopy. Beideck et al. (1994) reported oscillator strengths for the individual lines of the multiplets at 1814 Å and 1299 Å obtained from the measured lifetimes and branching ratios using beam-foil spectroscopic techniques. Bridges & Wiese (1967) measured transition probabilities in

Table 1
Measurement and Instrument Configuration Parameters

Spectral Range (cm^{-1})	Resolution (cm^{-1})	Windows	Detector	Beam Splitter	Lens	Filter	
						CWL (μm)	BW (μm)
700 to 2000	0.04	KBr	MCT	KBr	ZnSe	no filter	
2000 to 5700	0.05	CaF ₂	InSb	CaF ₂	CaF ₂	3.75	2.50
5000 to 7000	0.05	CaF ₂	InSb	CaF ₂	CaF ₂	1.71	0.57
7000 to 11000	0.05	CaF ₂	InSb	CaF ₂	CaF ₂	no filter	

the visible region of the spectrum. Radiative lifetimes of excited S I states were reported by Berzinsh et al. (1997), who used time-resolved laser spectroscopy. These data were combined by Biémont et al. (1998) with their theoretical branching ratios to deduce a consistent set of f -values for vacuum ultraviolet (VUV) lines of S I.

Using the Atomic Spectra Database (ASD) of the National Institute of Standards and Technology (NIST), Kramida et al. (2023) presents transition probability data for all ionic states of the sulfur atom critically compiled by Podobedova et al. (2009). They have included recommended experimental and theoretical data from Beideck et al. (1994), Biémont et al. (1996, 1998), Froese Fischer et al. (2006), Müller (1968), Wiese et al. (1969), Zerme et al. (1997), and Zatsarinsky & Bartschat (2006). Besides transition probabilities, the NIST ASD also includes the critically evaluated data on S I energy levels from Martin et al. (1990) and the list of observed wavelengths and energy-level classifications of observed S I spectral lines from Kaufman & Martin (1993). These data are heavily based on the observations of the S I VUV spectrum by Kaufman (1982), but also include older data of Frerichs (1933), Meißner et al. (1933), and Jakobsson (1967) in the visible and infrared (IR) regions, as well as other studies by Tondello (1972), Alder et al. (1978), Eriksson (1978), Sarma & Joshi (1984), Gibson et al. (1986), Joshi et al. (1987), Pratt (1988), and Haas et al. (1991). Despite the large volume of available spectral data on S I, there are many deficiencies in the data presently recommended by the NIST ASD (Kramida et al. 2023). Specifically for the IR region, most available observations are of low and moderate accuracy, and many theoretically predicted transitions have not been observed. The energy levels compiled by Martin et al. (1990) have never been optimized to fit the entire set of observed wavelengths. Therefore, the accuracy of Ritz wavelengths computed from the available energy levels is rather poor, precluding an accurate analysis of observed astrophysical spectra, such as the IR solar spectrum recorded by the Atmospheric Chemistry Experiment (ACE; Hase et al. 2010).

The importance of accurately evaluated data on wavelengths and energy levels of atoms cannot be overstated given the huge amount of astrophysical observational data recorded by ground and space telescopes. Interpretation of these observational data requires accurately evaluated wavelengths and energy levels of atoms resulting from high-precision laboratory measurements. The aim of this paper is to present a compilation of existing data on wavelengths and energy levels of atomic sulfur, augmented with our additional observations. Given the fact that the available bibliography lacks works reporting measurements in the IR region for wavelengths longer than $3.5 \mu\text{m}$, we extend these data by analyzing our newly measured S I spectra in the IR domain using an infrared Fourier transform spectrometer (IR FTS).

The primary objective of our study is to acquire high-precision laboratory measurements of atomic sulfur lines in the IR region, ranging from 800 to 11,000 cm^{-1} . These lines correspond to the energy transitions between atomic sulfur energy levels with principal quantum numbers n ranging from 5 to 7, and orbital quantum numbers $l \geq 3$. These transitions are spread out over a broad range of IR wavelengths. The IR FTS provides a consistent high resolution and allows for a higher energy throughput, meaning it can measure more precise and accurate energy values for the levels of atomic sulfur (S I) compared to measurements conducted several decades ago using grating spectrographs in the UV and visible ranges. The previous research conducted by the authors (Civiš et al. 2012a, 2012b, 2012c, 2013, 2018; Kubelík et al. 2015) has demonstrated the effectiveness of using of IR FTS in finding new $l \geq 3$ levels, as well as in refining the existing levels of a number of atomic species.

2. Experimental Setup

In this study, a microwave (MW) discharge has been used to generate emission lines of sulfur in a helium buffer gas. Measurements were performed in a quartz tube with KBr and CaF₂ windows located at the ends of the tube. This enables spectra to be obtained in two ranges: (700–5000) cm^{-1} and (1800–11,000) cm^{-1} using two liquid-nitrogen-cooled detectors, HgCdTe (MCT) and InSb, respectively, for each measurement range. It should be noted that each detector had a different sensitivity. To cover the spectral range from 2000 to 7000 cm^{-1} , we used several bandpass interference filters, procured from Northumbria Optical Coatings Limited,⁴ UK. The parameters of measurements and instrument configuration for each measurement are listed in Table 1. The spectral regions with the wavenumbers lower than 2000 cm^{-1} and higher than 7000 cm^{-1} were measured without interference filters.

A plasma discharge in a He (99.996 %) flow was held at a pressure of (93–200) Pa (0.7 Torr–1.5 Torr) with Microtron 200 W unit at 2.45 GHz (70 W) as a source of MW. The pressure in the discharge cell needed to be slightly adjusted after initiation of the MW discharge. Over the course of the experiment, conditions within the discharge cell changed over time, with sulfur diffusing into the cooler edges of the chamber. When igniting the discharge, it was necessary to optimize the pressure of helium considering the ease of ignition and stabilization of the MW power at an optimal value. As our sample, we used sulfur powders with a purity level of 99.99%. The observed spectra show traces of impurities such as oxygen, nitrogen, and argon in our discharge plasma.

⁴ The identification of commercial products in this paper does not imply recommendation or endorsement by the National Institute of Standards and Technology, nor does it imply that the items identified are necessarily the best available for the purpose.

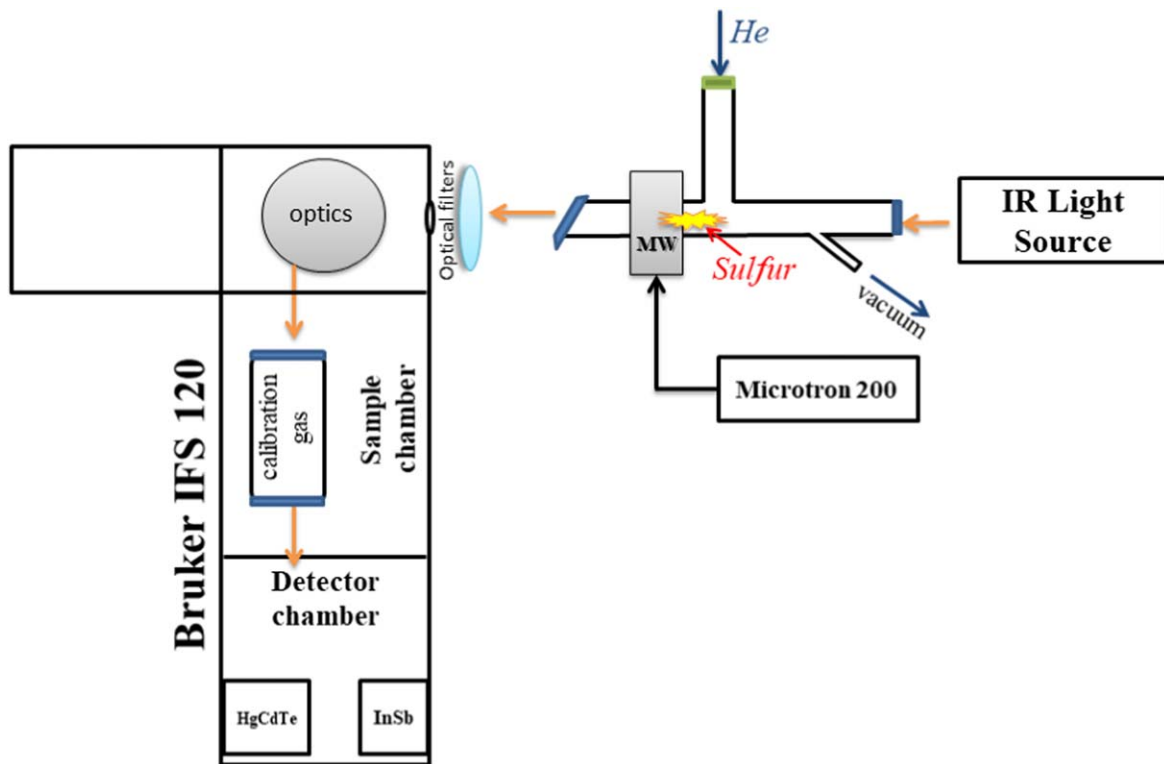


Figure 1. Scheme of the experimental setup with the microwave discharge.

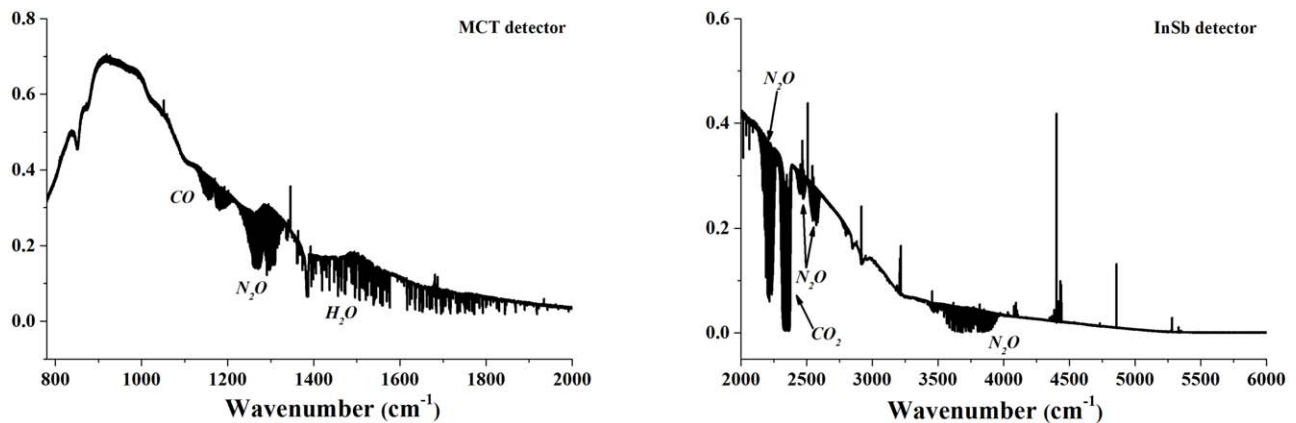


Figure 2. Sulfur emission spectra containing N_2O molecular absorption lines which were used for the calibration. Intensities on the vertical axes are in arbitrary units proportional to energy flux per unit wavenumber.

IR FTS measurements were performed using a Bruker IFS 120 setup, using the abovementioned detectors and the OPUS software (OPUS 2004), which allowed for adjustments to the necessary aperture, resolution, phase correction parameters, as well as optical and electronic filters. In order to obtain reliable results, multiple series of sulfur measurements were conducted, with sulfur samples and optical windows (KBr and CaF_2) being replaced in each instance. This was due to the windows becoming coated with sulfur layers during extended measurements in the He plasma discharge, resulting in reduced signal intensity. To enhance the signal-to-noise ratio, 100 scans were carried out for the examined range.

For the wavenumber calibration, we put a glass cell (equipped with KBr or CaF_2 windows) filled with a calibration gas in the spectrometer's sample chamber (between the detector

and the beam splitter, see Figure 1). The gases used for the wavenumber calibration were CO, H_2O and CH_4 . An additional IR radiation source (Thorlabs SLS203L/M) was utilized to enable the simultaneous measurement of the molecular absorption lines besides the atomic emission lines. For IR FTS measurement of the molecular lines, we used the technique described in our earlier works (Papoušek et al. 1991; Civiš et al. 2016). Examples of sulfur emission spectra containing molecular absorption lines are presented in Figure 2.

The wavenumbers were corrected by applying the following formula

$$\sigma_{\text{corr}} = \sigma_{\text{obs}}(1 - \alpha) - \beta, \quad (1)$$

where σ_{corr} are the corrected wavenumbers, σ_{obs} are the observed wavenumbers, and α and β are parameters obtained by linear fitting

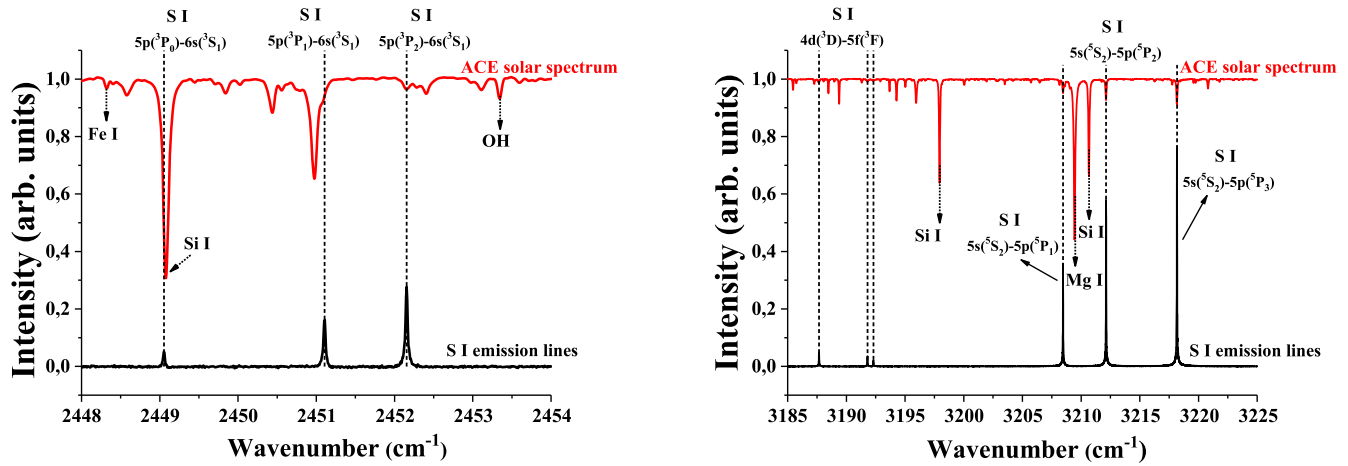


Figure 3. Comparison of emission spectra from S I plasma (lower plots) and the ACE Hase et al. (2010) solar spectra (upper red plots).

of the deviation between the line positions measured in this work and the high-precision wavenumbers taken from the HITRAN database (Gordon et al. 2022) as a function of wavenumber. The typical uncertainties of HITRAN wavenumbers are $\delta\sigma(\text{N}_2\text{O}) \approx (0.001\text{--}0.0001)\text{ cm}^{-1}$, $\delta\sigma(\text{CO}) \approx (0.00001\text{--}0.0001)\text{ cm}^{-1}$, and $\delta\sigma(\text{CH}_4) \approx (0.00001\text{--}0.001)\text{ cm}^{-1}$ ($\sigma < 1700\text{ cm}^{-1}$). The typical values of the calibration parameters α and β in Equation (1) for different bands are $\alpha = (1\text{--}2) \times 10^{-5}$ and $\beta = (2\text{--}3) \times 10^{-2}$, respectively, with the typical error values of $\delta\alpha = (1\text{--}2) \times 10^{-6}$ and $\delta\beta = (1\text{--}2) \times 10^{-3}$. In Fourier transform spectroscopy theory, the calibration normally is done with the help of the Equation (1) with $\beta = 0$; thus, its form with $\beta \neq 0$ is probably of no physical justification. Such a form is used as an option in Bruker software for the spectra analysis (OPUS 2004, Section 8.12). We retained the β term to account for possible systematic errors which could be due, for example, to a systematic phase shift in the interferogram (Brault 1987). We note that our interferograms were single-sided. Brault (1987) notes that such interferograms are sensitive to phase errors, which can be compensated with a nonzero β term in Equation (1).

3. Results and Discussion

The system of S I levels is similar to that of the first element of group VI, oxygen O I, which was described in our previous work (Civiš et al. 2018). The system of valence-excited S I levels is formed by configurations $3s^23p^4$, $3s3p^5$, and $3s^23p^3nl$ (henceforth, we will omit the closed $3s^2$ shell and use shortened designations in the text, such as $3p^4$ and $3p^3nl$; however, we will retain this subshell in the tables, where it is necessitated by the existence of observed transitions from the $3s3p^5$ configuration). The $3p^4$ configuration forms three terms: the ground triplet, 3P , and two singlet terms, 1D and 1S , with energies (relative to the ground $3p^4\ ^3P_2$ level) of 9238.609 cm^{-1} and $22,179.954\text{ cm}^{-1}$ (Kramida et al. 2023). The maximum percentage (57–58) % of the $3s3p^5$ configuration characterizes the $^3P^o$ levels with energies about $72,000\text{ cm}^{-1}$. All our observed lines of S I correspond to transitions between the excited levels that belong to the $3p^3nl$ configurations. They can be treated as excitations of one- p -electron states with the principal and orbital quantum numbers $n \geq 4$ and $l \geq 0$, respectively. The $3p^3$ ionic core configuration can form three terms: $^4S^o$, $^2D^o$, and $^2P^o$. Hereafter, the excited levels corresponding to these three terms are called normal, first-

and second-excited term systems. Only two second-excited terms, $3p^3(^2P^o)4s\ ^3P^o$ and $3p^3(^2P^o)4s\ ^1P^o$ lie below the first ionization limit (the triplet near $77,150\text{ cm}^{-1}$ and the singlet at $77,288\text{ cm}^{-1}$); we did not observe any transitions involving these levels. As for the first-excited terms, those lying below the first ionization limit are (Kramida et al. 2023): $3p^3(^2D^o)4s\ ^1,^3D^o$ (the triplet between $67,816\text{ cm}^{-1}$ and $67,842\text{ cm}^{-1}$, and the singlet at $69,237\text{ cm}^{-1}$), $3p^3(^2D^o)4p\ ^1,^3P$ (the triplet between $79,385\text{ cm}^{-1}$ and $79,418\text{ cm}^{-1}$, and the singlet at $77,855\text{ cm}^{-1}$), $3p^3(^2D^o)4p\ ^3D$ (between $78,152\text{ cm}^{-1}$ and $78,203\text{ cm}^{-1}$), $3p^3(^2D^o)4p\ ^1,^3F$ (between $78,400\text{ cm}^{-1}$ and $78,640\text{ cm}^{-1}$), $3p^3(^2D^o)3d\ ^1P^o$ at $81,438\text{ cm}^{-1}$ and $3p^3(^2D^o)(^2D^o)3d\ ^1F^o$ at $82,604\text{ cm}^{-1}$. We observed nine lines corresponding to transitions between the levels of the first-excited system and 12 lines of the transitions between the first-excited and the normal system. The rest of our observed emission lines are due to transitions between the normal system terms, which, in turn, are subdivided into two groups of triplet($3p^3nl\ ^3L$) and quintet($3p^3nl\ ^5L$) terms. Since the $3p^3$ ionic core term of the normal system is $^4S^o$, one has $L = l$ in the LS coupling scheme.

3.1. Observed S I Lines

As an example, Figure 3 shows the most prominent S I emission lines in ranges near 2500 cm^{-1} and 3200 cm^{-1} together with ACE solar spectra (Hase et al. 2010). Most of our intense emission peaks are lined up with the closest S I features listed in this atlas.

Because the levels with high orbital quantum number, $l > 4$ are absent in the available line lists, we started from approximated energies of the g , h , and i levels obtained with the Rydberg formula

$$E_{nl} = \text{IE} - \frac{R_s}{(n - \mu_{nl})^2}, \quad (2)$$

with small quantum defects, $\mu_{nl} \approx 0.001$ to identify the lines involving these levels (in Equation (2), $\text{IE} = 83,559.1\text{ cm}^{-1}$ is the ionization energy (IE) of S I (Kramida et al. 2023), $R_s = 109,735.438\text{ cm}^{-1}$ is the Rydberg constant of the S atom). After the designation of the lines involving these previously unknown levels, their energies (and therefore quantum defects) are refined in the optimization procedure (see Section 3.2) using the measured line wavenumbers. Identifications of the lines were assisted by the oscillator strengths calculated using

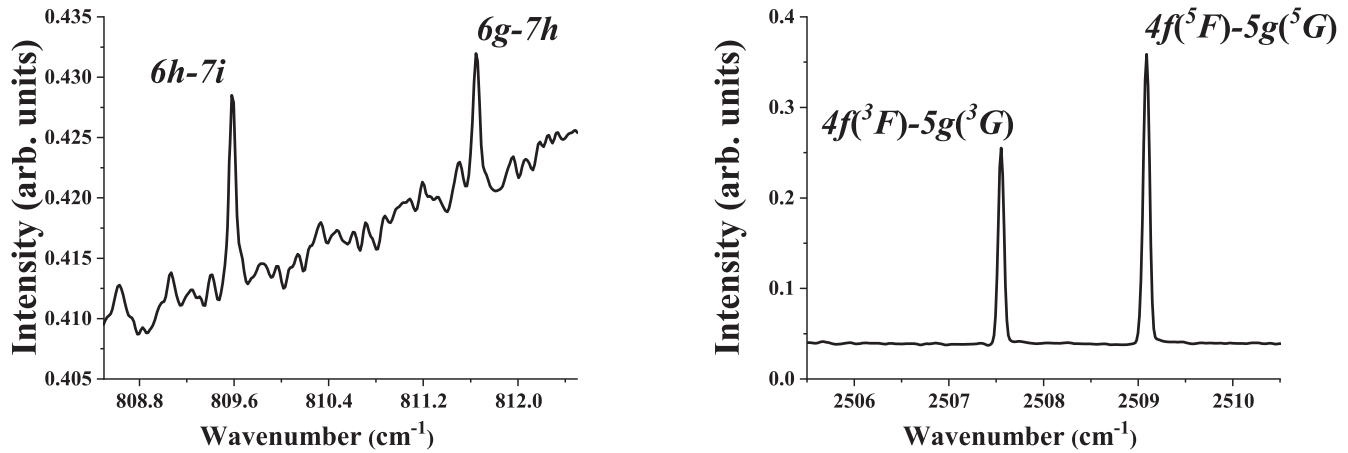


Figure 4. Some examples of the recorded S I spectra.

the single-channel quantum defect theory (QDT; see Seaton 1983; Chernov et al. 2000).

Some examples of the S I spectra recorded in our study are shown in the figures below. Figure 4 shows several lines that have never been reported before, including the $6h-7i$ and $6g-7h$ transitions (near 810 cm^{-1}) and the $4f-5g$ transitions (near 2500 cm^{-1}). The observed high intensity of the abovementioned transitions can easily be explained in the QDT framework. Indeed, the QDT wave function has n_r nodes outside the atomic core where the “radial” quantum number, n_r , is the closest integer to $n-l-1$. The transition probability (as well as oscillator or line strength) is proportional to the squared radial matrix element, $|\langle n'l|r|n''l''\rangle|^2$. For given n', n'' (which determine approximate transition wavenumber according to the Rydberg formula (2)), the radial integral is maximal when the number of nodes, n_r , is minimal for both integrands (i.e., the wave functions of the $|n'l'\rangle$ and $|n''l''\rangle$ states). As can be easily seen, $n-l-1=0$ for $4f, 5g, 6h,$ and $7i$ states, and $n-l-1=1$ for $6g$ and $7h$ states.

In Table 2 we present a data set comprising 172 atomic sulfur lines observed in our experiment in the IR region between 800 and $11,000\text{ cm}^{-1}$ including 87 previously unreported line features. Table 2 also provides crucial line parameters such as wavenumbers of the line positions, intensities, and line widths. These parameters were obtained by fitting the experimental spectra with Lorentzian or Gaussian profiles, whichever provided a better fit. The measurements were performed in different spectral ranges (corresponding to the abovementioned bandpass interference filters): from 800 to 2000 cm^{-1} , from 2000 to 5300 cm^{-1} , from 5300 to 7000 cm^{-1} , and from 7000 to $11,000\text{ cm}^{-1}$. The range from 5300 to 7000 cm^{-1} is further separated into three subranges, which were recorded in different experiments. These ranges are divided in Table 2 by mid-page horizontal lines. Since radiometric calibration in different spectral ranges is a difficult task, the recorded relative intensities are not on a coherent scale. Therefore, the arbitrary units of intensity specified in Table 2 are valid only within the same spectral range. The given intensities are integrated energy fluxes under the line profile. Their estimated relative accuracy (within each spectral range) is expected to be about 30 % for strong isolated lines but can be significantly worse for weaker and blended lines. No account was made for possible effects of self-absorption and nonuniformity of the emitting plasma. In all tables, the uncertainties are reported in parentheses immediately following

the values. They should be treated as the uncertainties in the rightmost significant digits, e.g., $123.4(56)$ means 123.4 ± 5.6 . The uncertainties (on the level of one standard deviation) of the measured lines presented in Table 2 were calculated by adding the statistical and calibration uncertainties in quadrature: $\delta\sigma = \sqrt{(\delta\sigma_{\text{stat}})^2 + (\delta\alpha \cdot \sigma)^2 + (\delta\beta)^2}$. This approximation is justified by low correlation (of the order of 0.01) between α and β .

It has been brought to our attention that a discrepancy exists in the spectral data reported in the NIST ASD database Kramida et al. (2023) concerning the wavelength of 10633.080 \AA (in air). This wavelength is associated with the spectral line that uniquely defines the $3p^3(^2D^o)4p\ ^1F_3$ energy level and is referred to the work of Jakobsson (1967). It appears that the discrepancy originates from an error in Jakobsson’s (1967) original publication: while the correct air wavelength of 10635.993 \AA is reported therein, the corresponding observed wavenumber is erroneously listed as 9402.037 cm^{-1} (should be 9399.462 cm^{-1}). This error appears to stem from a miscalculation where the air wavelength was not converted to vacuum prior to derivation of the wavenumber.⁵ To definitively resolve the controversy associated with this spectral line, we have measured this part of the S I spectrum with our advanced resolution capabilities. The outcome is presented in Figure 5. Our measured data for this line are included in Table 2.

3.2. S I Energy Levels

To update the list of energy-level values of S I we used the LOPT program (Kramida 2011), which performs a least-squares fitting of energy levels to observed wavelengths. Like any regression model, the LOPT optimization procedure yields statistical uncertainties of the energy-level values extracted from the list of transitions whose wavenumbers have their own uncertainties. Although there is no rigorous procedure to account for systematic uncertainties, the LOPT program performs some estimation of the possible effects of systematic shifts, see Equations (22)–(26) in Kramida (2011). The accuracy of the fit depends on the quality and completeness of the input spectral lines used in the fitting procedure.

⁵ After this paper was submitted for publication, an anonymous reviewer notified us that there was a recent paper of Ryde et al. (2019) investigating this line in stellar and solar spectra. We did not know about that work, but our independent findings are in complete agreement with the analysis of Ryde et al. (2019).

Table 2
S I Measured IR Line Wavenumbers (ν_{ki}), Relative Intensities (I_{ki}), Signal-to-Noise Ratios (SNR), and Full Widths at Half-maxima (FWHM)

This Work (cm^{-1})	Intensity (arb. units)	SNR	FWHM (cm^{-1})	Identification		Other Works (cm^{-1})
801.319(25)	2.5×10^{-4}	3.5	0.027	$3s^23p^3(^4S^o)6p^3P_2$	$3s^23p^3(^4S^o)5d^5D_3^o$...
809.593(10)	1.2×10^{-3}	10.0	0.042	$3s^23p^3(^4S^o)6h$	$3s^23p^3(^4S^o)7i$...
811.653(12)	8.7×10^{-4}	7.9	0.049	$3s^23p^3(^4S^o)6g$	$3s^23p^3(^4S^o)7h$...
871.925(42)	7.4×10^{-4}	2.6	0.106	$3s^23p^3(^4S^o)5d^5D_1^o$	$3s^23p^3(^4S^o)5f^5F_2$...
872.160(19)	5.6×10^{-4}	3.0	0.046	$3s^23p^3(^4S^o)5d^5D_2^o$	$3s^23p^3(^4S^o)5f^5F_{1,2}$...
872.479(24)	9.5×10^{-4}	4.1	0.060	$3s^23p^3(^4S^o)5d^5D_3^o$	$3s^23p^3(^4S^o)5f^5F_{2,3,4}$...
872.804(15)	6.4×10^{-4}	5.0	0.039	$3s^23p^3(^4S^o)5d^5D_4^o$	$3s^23p^3(^4S^o)5f^5F_{3,4,5}$...
1052.270(14)	2.6×10^{-3}	3.1	0.046	$3s^23p^3(^4S^o)5p^5P_3$	$3s^23p^3(^4S^o)4d^5D_4^o$	1052.267 H10u
1053.182(25)	4.7×10^{-4}	2.8	0.033	$3s^23p^3(^4S^o)5p^5P_3$	$3s^23p^3(^4S^o)4d^5D_3^o$...
1059.215(18)	1.8×10^{-3}	2.0	0.053	$3s^23p^3(^4S^o)5p^5P_2$	$3s^23p^3(^4S^o)4d^5D_3^o$...
1060.253(15)	6.3×10^{-4}	3.3	0.042	$3s^23p^3(^4S^o)5p^5P_2$	$3s^23p^3(^4S^o)4d^5D_2^o$...
1063.914(22)	8.0×10^{-4}	2.5	0.071	$3s^23p^3(^4S^o)5p^5P_1$	$3s^23p^3(^4S^o)4d^5D_2^o$...
1064.844(24)	6.5×10^{-4}	1.9	0.047	$3s^23p^3(^4S^o)5p^5P_1$	$3s^23p^3(^4S^o)4d^5D_1^o$...
1169.852(25)	6.9×10^{-4}	2.4	0.029	$3s^23p^3(^4S^o)6s^3S_1^o$	$3s^23p^3(^4S^o)6p^3P_2$...
1192.852(15)	1.0×10^{-3}	3.1	0.046	$3s^23p^3(^4S^o)6s^3S_1^o$	$3s^23p^3(^4S^o)6p^3P_1$...
1201.500(22)	1.1×10^{-3}	4.1	0.057	$3s^23p^3(^4S^o)6p^3P_3$	$3s^23p^3(^4S^o)7s^3S_2^o$...
1345.892(5)	9.2×10^{-3}	24.1	0.045	$3s^23p^3(^4S^o)5g$	$3s^23p^3(^4S^o)6h$...
1364.346(8)	2.5×10^{-3}	14.2	0.049	$3s^23p^3(^4S^o)5f^5F_{1,2,3,4,5}$	$3s^23p^3(^4S^o)6g$...
1386.764(42)	3.8×10^{-4}	2.1	0.030	$3s^23p^3(^4S^o)6s^3S_2^o$	$3s^23p^3(^4S^o)6p^5P_1$...
1389.239(18)	1.4×10^{-3}	4.4	0.039	$3s^23p^3(^4S^o)6s^3S_2^o$	$3s^23p^3(^4S^o)6p^5P_2$...
1392.463(7)	1.9×10^{-3}	12.2	0.041	$3s^23p^3(^4S^o)6s^3S_2^o$	$3s^23p^3(^4S^o)6p^5P_3$...
1678.178(21)	8.4×10^{-4}	3.5	0.090	$3s^23p^3(^4S^o)4d^5D_0^o$	$3s^23p^3(^4S^o)4f^5F_1$...
1678.724(11)	1.2×10^{-3}	4.5	0.067	$3s^23p^3(^4S^o)4d^5D_1^o$	$3s^23p^3(^4S^o)4f^5F_2$...
1679.620(28)	1.7×10^{-3}	2.7	0.054	$3s^23p^3(^4S^o)4d^5D_2^o$	$3s^23p^3(^4S^o)4f^5F_3$...
1680.155(37)	1.1×10^{-3}	2.5	0.075	$3s^23p^3(^4S^o)5p^3P_0$	$3s^23p^3(^4S^o)4d^3D_1^o$...
1680.646(23)	2.3×10^{-3}	3.8	0.050	$3s^23p^3(^4S^o)4d^5D_3^o$	$3s^23p^3(^4S^o)4f^5F_4$	1680.641 H10u
1681.546(6)	2.9×10^{-3}	14.1	0.045	$3s^23p^3(^4S^o)4d^5D_4^o$	$3s^23p^3(^4S^o)4f^5F_5$	1681.546 H10u
1682.729(21)	1.2×10^{-3}	3.2	0.041	$3s^23p^3(^4S^o)5p^3P_1$	$3s^23p^3(^4S^o)4d^3D_2^o$	1682.719 H10u
1687.889(6)	2.7×10^{-3}	10.3	0.045	$3s^23p^3(^4S^o)5p^3P_2$	$3s^23p^3(^4S^o)4d^3D_3^o$	1687.883 H10u
1934.109(7)	1.2×10^{-3}	16.3	0.041	$3s^23p^3(^4S^o)4d^3D_3^o$	$3s^23p^3(^4S^o)6p^3P_2$	1934.056 H10
2035.124(13)	4.0×10^{-4}	4.1	0.061	$3s^23p^3(^4S^o)4f^3F_3$	$3s^23p^3(^4S^o)5d^3D_2^o$...
2035.548(13)	3.3×10^{-4}	5.7	0.055	$3s^23p^3(^4S^o)4f^3F_4$	$3s^23p^3(^4S^o)5d^3D_3^o$...
2036.236(62)	9.1×10^{-4}	2.0	0.213	$3s^23p^3(^4S^o)4f^3F_2$	$3s^23p^3(^4S^o)5d^3D_1^o$...
2135.545(12)	3.8×10^{-4}	7.3	0.058	$3s^23p^3(^4S^o)6p^5P_3$	$3s^23p^3(^4S^o)6d^5D_4^o$...
2138.943(16)	2.7×10^{-4}	6.3	0.054	$3s^23p^3(^4S^o)6p^5P_2$	$3s^23p^3(^4S^o)6d^5D_3^o$...
2154.967(6)	1.1×10^{-3}	17.0	0.059	$3s^23p^3(^4S^o)5g$	$3s^23p^3(^4S^o)7h$...
2173.031(25)	3.0×10^{-4}	2.8	0.063	$3s^23p^3(^4S^o)5f^5F_{2,3,4}$	$3s^23p^3(^4S^o)7g$...
2174.307(11)	5.8×10^{-4}	10.6	0.065	$3s^23p^3(^4S^o)5f^5F_{1,2,3,4,5}$	$3s^23p^3(^4S^o)7g$...
2449.068(12)	4.5×10^{-4}	7.8	0.056	$3s^23p^3(^4S^o)5p^3P_0$	$3s^23p^3(^4S^o)6s^3S_1^o$...
2451.115(7)	1.6×10^{-3}	9.9	0.056	$3s^23p^3(^4S^o)5p^3P_1$	$3s^23p^3(^4S^o)6s^3S_1^o$	2451.095 H10
2452.164(6)	2.7×10^{-3}	12.0	0.055	$3s^23p^3(^4S^o)5p^3P_2$	$3s^23p^3(^4S^o)6s^3S_1^o$	2452.158 H10
2507.566(6)	2.2×10^{-2}	10.3	0.060	$3s^23p^3(^4S^o)4f^5F_{2,3,4}$	$3s^23p^3(^4S^o)5g$...
2509.103(9)	3.7×10^{-2}	6.0	0.067	$3s^23p^3(^4S^o)4f^5F_{1,2,3,4,5}$	$3s^23p^3(^4S^o)5g$...
2543.044(6)	7.0×10^{-3}	11.0	0.057	$3s^23p^3(^4S^o)5p^5P_3$	$3s^23p^3(^4S^o)6s^3S_2^o$	2543.043 H10
2549.083(5)	5.0×10^{-3}	15.9	0.057	$3s^23p^3(^4S^o)5p^5P_2$	$3s^23p^3(^4S^o)6s^3S_2^o$	2549.080 H10
2552.751(5)	2.9×10^{-3}	26.0	0.056	$3s^23p^3(^4S^o)5p^5P_1$	$3s^23p^3(^4S^o)6s^3S_2^o$	2552.743 H10
2655.106(10)	3.4×10^{-4}	11.7	0.048	$3s^23p^3(^4S^o)6s^3S_1^o$	$3s^23p^3(^2D^o)4p^3P_2$	2655.126 H10u
2874.101(15)	2.2×10^{-4}	5.0	0.057	$3s^23p^3(^4S^o)4d^5D_0^o$	$3s^23p^3(^4S^o)6p^5P_1$	2874.100 H10u
2874.668(11)	3.7×10^{-4}	7.3	0.054	$3s^23p^3(^4S^o)4d^5D_1^o$	$3s^23p^3(^4S^o)6p^5P_1$...
2875.595(21)	2.3×10^{-4}	5.1	0.050	$3s^23p^3(^4S^o)4d^5D_2^o$	$3s^23p^3(^4S^o)6p^5P_1$...
2877.133(23)	2.7×10^{-4}	3.4	0.067	$3s^23p^3(^4S^o)4d^5D_1^o$	$3s^23p^3(^4S^o)6p^5P_2$	2877.215 H10u
2878.069(14)	6.7×10^{-4}	4.2	0.062	$3s^23p^3(^4S^o)4d^5D_2^o$	$3s^23p^3(^4S^o)6p^5P_2$	2878.063 H10u
2878.822(30)	3.1×10^{-4}	2.4	0.068	$3s^23p^3(^4S^o)4d^5D_1^o$	$3s^23p^3(^2D^o)4p^1P_1$...
2879.108(13)	1.1×10^{-3}	4.0	0.062	$3s^23p^3(^4S^o)4d^5D_3^o$	$3s^23p^3(^4S^o)6p^5P_2$...
2882.332(10)	6.2×10^{-4}	6.2	0.062	$3s^23p^3(^4S^o)4d^5D_3^o$	$3s^23p^3(^4S^o)6p^5P_3$	2882.314 H10u
2883.240(7)	2.1×10^{-3}	7.0	0.058	$3s^23p^3(^4S^o)4d^5D_4^o$	$3s^23p^3(^4S^o)6p^5P_3$	2883.237 H10u
2917.160(6)	2.5×10^{-2}	10.2	0.058	$3s^23p^3(^4S^o)5s^3S_1^o$	$3s^23p^3(^4S^o)5p^3P_2$	2917.143 J67, 2917.150 H10

Table 2
(Continued)

This Work (cm ⁻¹)	Intensity (arb. units)	SNR	FWHM (cm ⁻¹)	Identification		Other Works (cm ⁻¹)
2918.210(6)	1.5×10^{-2}	10.8	0.057	$3s^23p^3(4S^o)5s \ ^3S_1^o$	$3s^23p^3(4S^o)5p \ ^3P_1$	2918.192 J67, 2918.154 H10
2920.259(9)	5.0×10^{-3}	4.8	0.059	$3s^23p^3(4S^o)5s \ ^3S_1^o$	$3s^23p^3(4S^o)5p \ ^3P_0$	2920.251 J67, 2920.243 H10
2924.965(3)	2.2×10^{-4}	22.0	0.020	$3s^23p^3(4S^o)4p \ ^3P_0$	$3s^23p^3(2D^o)4s \ ^3D_1^o$	2924.966 H10u
2927.386(4)	1.1×10^{-4}	17.8	0.018	$3s^23p^3(4S^o)4p \ ^3P_1$	$3s^23p^3(2D^o)4s \ ^3D_1^o$	2927.412 H10u
2932.605(2)	2.5×10^{-4}	33.2	0.022	$3s^23p^3(4S^o)4p \ ^3P_2$	$3s^23p^3(2D^o)4s \ ^3D_2^o$	2932.602 H10u
2936.240(14)	3.1×10^{-4}	6.0	0.047	$3s^23p^3(4S^o)4p \ ^3P_1$	$3s^23p^3(2D^o)4s \ ^3D_2^o$...
2950.299(6)	1.6×10^{-3}	9.7	0.062	$3s^23p^3(4S^o)4p \ ^3P_2$	$3s^23p^3(2D^o)4s \ ^3D_3^o$	2950.293 H10
2997.447(17)	4.4×10^{-4}	5.4	0.061	$3s^23p^3(4S^o)4p \ ^3P_2$	$3s^23p^3(4S^o)3d \ ^5D_3^o$	2997.432 H10
3187.688(7)	2.7×10^{-3}	7.1	0.061	$3s^23p^3(4S^o)4d \ ^3D_3^o$	$3s^23p^3(4S^o)5f \ ^3F_4$	3187.670 H10
3191.814(7)	1.8×10^{-3}	9.5	0.059	$3s^23p^3(4S^o)4d \ ^3D_2^o$	$3s^23p^3(4S^o)5f \ ^3F_3$	3191.792 H10u
3192.320(8)	1.2×10^{-3}	6.3	0.063	$3s^23p^3(4S^o)4d \ ^3D_1^o$	$3s^23p^3(4S^o)5f \ ^3F_2$	3192.290 H10u
3208.477(5)	1.2×10^{-2}	29.0	0.057	$3s^23p^3(4S^o)5s \ ^5S_2^o$	$3s^23p^3(4S^o)5p \ ^5P_1$	3208.470 J67, 3208.471 H10
3212.145(6)	2.0×10^{-2}	10.5	0.059	$3s^23p^3(4S^o)5s \ ^5S_2^o$	$3s^23p^3(4S^o)5p \ ^5P_2$	3212.137 J67, 3212.132 H10
3218.184(5)	2.7×10^{-2}	17.7	0.058	$3s^23p^3(4S^o)5s \ ^5S_2^o$	$3s^23p^3(4S^o)5p \ ^5P_3$	3218.174 J67, 3218.172 H10
3285.850(6)	1.1×10^{-4}	14.0	0.028	$3s^23p^3(2D^o)4p \ ^3D_1$	$3s^23p^3(2D^o)3d \ ^1P_1^o$...
3583.303(9)	5.9×10^{-4}	12.9	0.056	$3s^23p^3(2D^o)4p \ ^1P_1$	$3s^23p^3(2D^o)3d \ ^1P_1^o$...
3850.876(6)	2.5×10^{-3}	13.0	0.066	$3s^23p^3(4S^o)4f \ ^5F_{2,3,4}$	$3s^23p^3(4S^o)6g$	3850.883 H10u
3852.414(5)	2.5×10^{-3}	19.9	0.071	$3s^23p^3(4S^o)4f \ ^5F_{1,2,3,4,5}$	$3s^23p^3(4S^o)6g$	3852.380 H10u
4094.606(6)	1.5×10^{-2}	9.3	0.063	$3s^23p^3(4S^o)3d \ ^3D_3^o$	$3s^23p^3(4S^o)5p \ ^3P_2$	4094.589 J67, 4094.597 H10
4102.379(5)	2.6×10^{-3}	22.1	0.061	$3s^23p^3(4S^o)3d \ ^3D_2^o$	$3s^23p^3(4S^o)5p \ ^3P_2$	4102.391 H10
4103.429(7)	7.9×10^{-3}	6.7	0.063	$3s^23p^3(4S^o)3d \ ^3D_2^o$	$3s^23p^3(4S^o)5p \ ^3P_1$	4103.422 H10
4104.968(8)	2.8×10^{-3}	6.2	0.065	$3s^23p^3(4S^o)3d \ ^3D_1^o$	$3s^23p^3(4S^o)5p \ ^3P_1$	4104.959 J67, 4104.952 H10
4107.019(5)	3.4×10^{-3}	14.3	0.063	$3s^23p^3(4S^o)3d \ ^3D_1^o$	$3s^23p^3(4S^o)5p \ ^3P_0$	4107.002 J67, 4107.026 H10
4156.388(25)	3.6×10^{-4}	4.8	0.080	$3s^23p^3(4S^o)4d \ ^3D_3^o$	$3s^23p^3(4S^o)7p \ ^3P_2$...
4166.776(17)	2.4×10^{-4}	5.7	0.055	$3s^23p^3(4S^o)4d \ ^5D_1^o$	$3s^23p^3(4S^o)5f \ ^5F_2$	4166.769 H10u
4167.699(7)	7.3×10^{-4}	9.4	0.072	$3s^23p^3(4S^o)4d \ ^5D_2^o$	$3s^23p^3(4S^o)5f \ ^5F_3$...
4168.720(8)	9.6×10^{-4}	8.7	0.063	$3s^23p^3(4S^o)4d \ ^5D_3^o$	$3s^23p^3(4S^o)5f \ ^5F_4$...
4169.610(7)	1.2×10^{-3}	9.0	0.062	$3s^23p^3(4S^o)4d \ ^5D_4^o$	$3s^23p^3(4S^o)5f \ ^5F_5$...
4349.072(11)	4.8×10^{-3}	4.1	0.067	$3s^23p^3(4S^o)5p \ ^5P_3$	$3s^23p^3(4S^o)5d \ ^5D_4^o$	4349.063 J67, 4349.093 H10
4349.414(13)	9.3×10^{-4}	6.0	0.057	$3s^23p^3(4S^o)5p \ ^5P_3$	$3s^23p^3(4S^o)5d \ ^5D_3^o$	4349.43 J67
4355.455(9)	2.3×10^{-3}	6.0	0.065	$3s^23p^3(4S^o)5p \ ^5P_2$	$3s^23p^3(4S^o)5d \ ^5D_3^o$	4355.60 J67, 4355.450 H10u
4355.789(14)	1.5×10^{-3}	2.9	0.068	$3s^23p^3(4S^o)5p \ ^5P_2$	$3s^23p^3(4S^o)5d \ ^5D_2^o$...
4356.032(28)	4.0×10^{-4}	2.7	0.059	$3s^23p^3(4S^o)5p \ ^5P_2$	$3s^23p^3(4S^o)5d \ ^5D_1^o$...
4359.451(13)	6.8×10^{-4}	4.2	0.058	$3s^23p^3(4S^o)5p \ ^5P_1$	$3s^23p^3(4S^o)5d \ ^5D_2^o$...
4359.704(19)	1.5×10^{-3}	2.5	0.077	$3s^23p^3(4S^o)5p \ ^5P_1$	$3s^23p^3(4S^o)5d \ ^5D_1^o$	4359.61 J67
4359.859(34)	4.2×10^{-4}	2.6	0.059	$3s^23p^3(4S^o)5p \ ^5P_1$	$3s^23p^3(4S^o)5d \ ^5D_0^o$...
4367.829(11)	8.1×10^{-3}	4.0	0.068	$3s^23p^3(4S^o)4p \ ^5P_3$	$3s^23p^3(2D^o)4s \ ^3D_3^o$	4367.817 J67, 4367.790 H10
4368.061(19)	1.9×10^{-3}	2.7	0.072	$3s^23p^3(4S^o)4p \ ^5P_2$	$3s^23p^3(2D^o)4s \ ^3D_2^o$	4368.06 J67, 4368.048 H10
4370.333(25)	4.2×10^{-4}	3.8	0.115	$3s^23p^3(4S^o)4p \ ^5P_1$	$3s^23p^3(2D^o)4s \ ^3D_1^o$	4370.271 J67
4379.138(6)	9.1×10^{-4}	20.1	0.061	$3s^23p^3(4S^o)4p \ ^5P_1$	$3s^23p^3(2D^o)4s \ ^3D_2^o$	4379.122 J67
4385.737(8)	1.6×10^{-2}	6.5	0.064	$3s^23p^3(4S^o)4p \ ^5P_2$	$3s^23p^3(2D^o)4s \ ^3D_3^o$	4385.725 J67, 4385.709 H10
4402.602(6)	2.0×10^{-1}	9.2	0.064	$3s^23p^3(4S^o)4p \ ^5P_3$	$3s^23p^3(4S^o)3d \ ^5D_4^o$	4402.584 J67, 4402.592 H10
4412.762(5)	5.1×10^{-3}	13.9	0.062	$3s^23p^3(4S^o)4p \ ^5P_3$	$3s^23p^3(4S^o)3d \ ^5D_2^o$	4412.746 J67, 4412.722 H10
4414.975(5)	3.0×10^{-2}	14.0	0.063	$3s^23p^3(4S^o)4p \ ^5P_3$	$3s^23p^3(4S^o)3d \ ^5D_3^o$	4414.958 J67, 4414.940 H10
4420.938(24)	1.6×10^{-4}	4.1	0.057	$3s^23p^3(4S^o)5p \ ^3P_0$	$3s^23p^3(4S^o)5d \ ^3D_1^o$...
4421.866(15)	2.9×10^{-4}	6.3	0.056	$3s^23p^3(4S^o)5p \ ^3P_1$	$3s^23p^3(4S^o)5d \ ^3D_2^o$...
4423.321(11)	5.6×10^{-4}	10.4	0.060	$3s^23p^3(4S^o)5p \ ^3P_2$	$3s^23p^3(4S^o)5d \ ^3D_3^o$...
4428.401(8)	1.5×10^{-2}	6.2	0.065	$3s^23p^3(4S^o)4p \ ^5P_2$	$3s^23p^3(4S^o)3d \ ^5D_1^o$	4428.386 J67
4430.671(5)	4.5×10^{-2}	15.0	0.063	$3s^23p^3(4S^o)4p \ ^5P_2$	$3s^23p^3(4S^o)3d \ ^5D_2^o$	4430.655 J67
4432.884(5)	6.0×10^{-2}	20.8	0.063	$3s^23p^3(4S^o)4p \ ^5P_2$	$3s^23p^3(4S^o)3d \ ^5D_3^o$	4432.866 J67
4438.109(6)	2.2×10^{-2}	9.5	0.064	$3s^23p^3(4S^o)4p \ ^5P_1$	$3s^23p^3(4S^o)3d \ ^5D_0^o$	4438.093 J67
4439.479(5)	4.3×10^{-2}	14.4	0.063	$3s^23p^3(4S^o)4p \ ^5P_1$	$3s^23p^3(4S^o)3d \ ^5D_1^o$	4439.462 J67
4441.749(6)	2.7×10^{-2}	9.7	0.064	$3s^23p^3(4S^o)4p \ ^5P_1$	$3s^23p^3(4S^o)3d \ ^5D_2^o$	4441.733 J67
4538.795(12)	7.5×10^{-4}	10.6	0.062	$3s^23p^3(4S^o)4d \ ^3D_3^o$	$3s^23p^3(4S^o)6f \ ^3F_4$...
4542.902(18)	6.5×10^{-4}	7.7	0.067	$3s^23p^3(4S^o)4d \ ^3D_2^o$	$3s^23p^3(4S^o)6f \ ^3F_3$...
4543.428(33)	5.1×10^{-4}	4.9	0.100	$3s^23p^3(4S^o)4d \ ^3D_1^o$	$3s^23p^3(4S^o)6f \ ^3F_2$...
4660.848(9)	5.2×10^{-4}	12.5	0.071	$3s^23p^3(4S^o)4f \ ^5F_{2,3,4}$	$3s^23p^3(4S^o)7g$...

Table 2
(Continued)

This Work (cm ⁻¹)	Intensity (arb. units)	SNR	FWHM (cm ⁻¹)	Identification		Other Works (cm ⁻¹)
4662.375(9)	5.6×10^{-4}	12.5	0.067	$3s^23p^3(^4S^o)4f^5F_{1,2,3,4,5}$	$3s^23p^3(^4S^o)7g$...
5137.019(12)	4.8×10^{-4}	7.5	0.080	$3s^23p^3(^4S^o)5p^5P_3$	$3s^23p^3(^4S^o)7s^5S_2^o$...
5143.062(18)	2.2×10^{-4}	6.3	0.058	$3s^23p^3(^4S^o)5p^5P_2$	$3s^23p^3(^4S^o)7s^5S_2^o$...
5146.734(24)	1.8×10^{-4}	4.1	0.062	$3s^23p^3(^4S^o)5p^5P_1$	$3s^23p^3(^4S^o)7s^5S_2^o$...
5273.254(10)	3.7×10^{-3}	7.3	0.067	$3s^23p^3(^4S^o)4p^3P_0$	$3s^23p^3(^4S^o)3d^3D_1^o$	5273.23 J67
5273.595(8)	4.4×10^{-3}	8.4	0.070	$3s^23p^3(^4S^o)4p^3P_2$	$3s^23p^3(^4S^o)3d^3D_2^o$	5273.58 J67
5275.677(6)	2.8×10^{-3}	12.6	0.066	$3s^23p^3(^4S^o)4p^3P_1$	$3s^23p^3(^4S^o)3d^3D_1^o$	5275.685 J67
5277.215(4)	1.3×10^{-2}	28.3	0.067	$3s^23p^3(^4S^o)4p^3P_1$	$3s^23p^3(^4S^o)3d^3D_2^o$	5277.223 J67
5281.378(5)	5.3×10^{-2}	19.5	0.067	$3s^23p^3(^4S^o)4p^3P_2$	$3s^23p^3(^4S^o)3d^3D_3^o$	5281.378 J67
5352.962(13)	2.5×10^5	5.7	0.032	$3s^23p^3(^4S^o)4d^3D_3^o$	$3s^23p^3(^4S^o)7f^3F_4$...
5357.052(19)	1.8×10^5	4.4	0.040	$3s^23p^3(^4S^o)4d^3D_2^o$	$3s^23p^3(^4S^o)7f^3F_3$...
5518.196(21)	2.2×10^5	5.6	0.054	$3s^23p^3(^4S^o)4d^5D_1^o$	$3s^23p^3(^4S^o)6f^5F_2$...
5519.118(13)	4.7×10^5	6.8	0.065	$3s^23p^3(^4S^o)4d^5D_2^o$	$3s^23p^3(^4S^o)6f^5F_3$...
5520.145(8)	5.7×10^5	9.6	0.051	$3s^23p^3(^4S^o)4d^5D_3^o$	$3s^23p^3(^4S^o)6f^5F_4$...
5521.047(5)	7.3×10^5	12.5	0.055	$3s^23p^3(^4S^o)4d^5D_4^o$	$3s^23p^3(^4S^o)6f^5F_5$...
6023.453(11)	1.3×10^{-3}	5.1	0.075	$3s^23p^3(^4S^o)3d^5D_2^o$	$3s^23p^3(^4S^o)5p^5P_1$	6023.453 J67
6024.904(13)	3.0×10^{-3}	3.7	0.073	$3s^23p^3(^4S^o)3d^5D_3^o$	$3s^23p^3(^4S^o)5p^5P_2$	6024.922 J67
6025.718(12)	1.7×10^{-3}	4.1	0.073	$3s^23p^3(^4S^o)3d^5D_1^o$	$3s^23p^3(^4S^o)5p^5P_1$	6025.734 J67
6027.108(6)	2.9×10^{-3}	13.2	0.076	$3s^23p^3(^4S^o)3d^5D_0^o$	$3s^23p^3(^4S^o)5p^5P_1$	6027.128 J67
6029.395(11)	6.6×10^{-4}	8.0	0.081	$3s^23p^3(^4S^o)3d^5D_1^o$	$3s^23p^3(^4S^o)5p^5P_2$...
6030.943(10)	1.2×10^{-3}	9.6	0.069	$3s^23p^3(^4S^o)3d^5D_3^o$	$3s^23p^3(^4S^o)5p^5P_3$	6030.943 J67
6043.322(5)	6.6×10^{-3}	15.1	0.073	$3s^23p^3(^4S^o)3d^5D_4^o$	$3s^23p^3(^4S^o)5p^5P_3$	6043.325 J67
6458.811(2)	1.5×10^8	18.1	0.043	$3s^23p^3(^4S^o)4p^3P_2$	$3s^23p^3(^4S^o)5s^3S_1^o$	6458.816 J67
6460.010(2)	2.9×10^7	36.2	0.042	$3s^23p^3(^4S^o)4p^3P_0$	$3s^23p^3(^4S^o)5s^3S_0^o$	6460.014 J67
6462.431(2)	8.8×10^7	18.4	0.043	$3s^23p^3(^4S^o)4p^3P_1$	$3s^23p^3(^4S^o)5s^3S_0^o$	6462.436 J67
6482.358(2)	1.2×10^8	27.8	0.046	$3s^23p^3(^4S^o)3d^3D_2^o$	$3s^23p^3(^4S^o)4f^3F_{3,4}$	6482.365 J67
6490.138(2)	8.6×10^7	35.0	0.052	$3s^23p^3(^4S^o)3d^3D_2^o$	$3s^23p^3(^4S^o)4f^3F_{2,3}$	6490.147 J67
6491.701(2)	5.2×10^7	39.8	0.045	$3s^23p^3(^4S^o)3d^3D_1^o$	$3s^23p^3(^4S^o)4f^3F_2$	6491.708 J67
7130.915(7)	4.3×10^{-4}	18.3	0.054	$3s^23p^3(^4S^o)4p^3P_2$	$3s3p^5^3P_2^o$	7130.911 J67
7227.740(4)	3.3×10^{-3}	26.9	0.058	$3s^23p^3(^4S^o)4p^5P_3$	$3s^23p^3(^4S^o)5s^5S_0^o$	7227.740 J67
7245.650(5)	2.3×10^{-3}	27.1	0.058	$3s^23p^3(^4S^o)4p^5P_2$	$3s^23p^3(^4S^o)5s^5S_0^o$	7245.648 J67
7256.731(5)	1.4×10^{-3}	35.0	0.057	$3s^23p^3(^4S^o)4p^5P_1$	$3s^23p^3(^4S^o)5s^5S_0^o$	7256.724 J67
7489.720(27)	7.4×10^{-5}	4.7	0.075	$3s^23p^3(^4S^o)4p^3P_2$	$3s3p^5^3P_1^o$	7489.747 J67
7493.334(33)	9.0×10^{-5}	4.4	0.074	$3s^23p^3(^4S^o)4p^3P_1$	$3s3p^5^3P_1^o$	7493.367 J67
8616.999(7)	3.6×10^{-4}	19.5	0.066	$3s^23p^3(^2D^o)4s^1D_2^o$	$3s^23p^3(^2D^o)4p^1P_1$	8617.017 J67
8764.767(5)	8.6×10^{-4}	25.9	0.064	$3s^23p^3(^4S^o)3d^3D_3^o$	$3s^23p^3(^4S^o)4f^5F_{3,4}$	8764.766 J67
8767.002(5)	7.1×10^{-4}	34.9	0.065	$3s^23p^3(^4S^o)3d^3D_2^o$	$3s^23p^3(^4S^o)4f^5F_{2,3}$	8767.004 J67
8769.294(8)	4.0×10^{-4}	14.5	0.062	$3s^23p^3(^4S^o)3d^5D_1^o$	$3s^23p^3(^4S^o)4f^5F_{1,2}$	8769.296 J67
8770.679(12)	1.1×10^{-4}	9.2	0.056	$3s^23p^3(^4S^o)3d^5D_0^o$	$3s^23p^3(^4S^o)4f^5F_1$	8770.689 J67
8777.140(5)	1.3×10^{-3}	24.1	0.060	$3s^23p^3(^4S^o)3d^5D_4^o$	$3s^23p^3(^4S^o)4f^5F_{4,5}$	8777.134 J67
8811.904(10)	1.7×10^{-4}	12.3	0.062	$3s^23p^3(^2D^o)4s^3D_3^o$	$3s^23p^3(^4S^o)4f^5F_{3,4}$	8811.907 J67
8970.172(12)	2.5×10^{-4}	11.8	0.071	$3s^23p^3(^4S^o)3d^3D_3^o$	$3s^23p^3(^4S^o)5f^3F_4$	8970.146 J67
8977.965(17)	1.5×10^{-4}	7.5	0.064	$3s^23p^3(^4S^o)3d^3D_2^o$	$3s^23p^3(^4S^o)5f^3F_{2,3}$	8977.932 J67
8979.496(32)	1.7×10^{-4}	5.7	0.139	$3s^23p^3(^4S^o)3d^3D_1^o$	$3s^23p^3(^4S^o)5f^3F_2$	8979.51 J67
9399.433(2)	2.5×10^{-4}	7.8	0.037	$3s^23p^3(^2D^o)4s^1D_2^o$	$3s^23p^3(^2D^o)4p^1F_3$	9402.037 J67, 9399.54 F33
9558.157(5)	5.0×10^{-3}	14.0	0.066	$3s^23p^3(^4S^o)4s^3S_1^o$	$3s^23p^3(^4S^o)4p^3P_1$	9558.153 J67, 9558.07 F33
9560.579(5)	1.6×10^{-3}	13.0	0.066	$3s^23p^3(^4S^o)4s^3S_0^o$	$3s^23p^3(^4S^o)4p^3P_0$	9560.575 J67, 9560.55 F33
9561.778(4)	1.0×10^{-2}	31.6	0.064	$3s^23p^3(^4S^o)4s^3S_0^o$	$3s^23p^3(^4S^o)4p^3P_2$	9561.769 J67, 9561.76 F33
10,326.878(7)	3.7×10^{-4}	19.6	0.066	$3s^23p^3(^2D^o)4s^3D_2^o$	$3s^23p^3(^2D^o)4p^3D_2$	10,326.883 J67, 10,326.87 F33
10,335.986(11)	2.0×10^{-4}	12.0	0.062	$3s^23p^3(^2D^o)4s^3D_1^o$	$3s^23p^3(^2D^o)4p^3D_1$	10,335.986 J67, 10,335.92 F33
10,360.317(4)	7.2×10^{-4}	34.7	0.066	$3s^23p^3(^2D^o)4s^3D_3^o$	$3s^23p^3(^2D^o)4p^3D_3$	10,360.317 J67, 10,359.94 F33
10,573.064(23)	1.4×10^{-4}	7.2	0.095	$3s^23p^3(^4S^o)3d^5D_3^o$	$3s^23p^3(^2D^o)4p^3F_4$	10,573.03 F33
10,593.601(11)	2.7×10^{-4}	14.1	0.078	$3s^23p^3(^2D^o)4s^3D_1^o$	$3s^23p^3(^2D^o)4p^3F_2$	10,593.56 F33
10,610.692(6)	4.1×10^{-4}	23.3	0.066	$3s^23p^3(^2D^o)4s^3D_2^o$	$3s^23p^3(^2D^o)4p^3F_3$	10,610.63 F33
10,620.261(4)	6.2×10^{-4}	39.2	0.065	$3s^23p^3(^2D^o)4s^3D_3^o$	$3s^23p^3(^2D^o)4p^3F_4$	10,620.17 F33

Table 2
(Continued)

This Work (cm^{-1})	Intensity (arb. units)	SNR	FWHM (cm^{-1})	Identification		Other Works (cm^{-1})
10,822.431(4)	2.1×10^{-3}	48.1	0.067	$3s^23p^3(^4S^{\circ})4s\ ^5S_2^{\circ}$	$3s^23p^3(^4S^{\circ})4p\ ^5P_1$	10,822.425 J67, 10,822.48 F33
10,833.513(4)	2.9×10^{-3}	42.4	0.066	$3s^23p^3(^4S^{\circ})4s\ ^5S_2^{\circ}$	$3s^23p^3(^4S^{\circ})4p^2P_2$	10,833.503 J67, 10,833.47 F33
10,851.425(4)	4.1×10^{-3}	62.5	0.067	$3s^23p^3(^4S^{\circ})4s\ ^5S_2^{\circ}$	$3s^23p^3(^4S^{\circ})4p\ ^5P_3$	10,851.409 J67, 10,851.35 F33

Note. Key to literature references: H10–Hase et al. (2010); H10u–unidentified line observed by Hase et al. (2010); F33–Frerichs (1933); J67–Jakobsson (1967).

Therefore, it is important to use as large as possible set of input lines to obtain the most accurate and reliable results. We have collected as much spectral data from literature as possible for the sulfur atom, restricted to laboratory observations only.

Although Table 2 contains 172 lines, only 152 of them (corresponding to 191 transitions) were used in the level optimization. The remaining 20 lines were previously measured by Jakobsson (1967) with somewhat smaller uncertainties; our general policy was to use the most accurate measurement for each line. We note that, although most of the lines observed with the FTS could be measured very precisely, a few very weak ones had a too low signal-to-noise ratio and could not be measured better than was possible for Jakobsson. The following list specifies the number of transitions included in the level optimization procedure from each source:

1. 191 IR transitions from the present work;
2. 237 UV transitions from Joshi et al. (1987), Sarma & Joshi (1984), Tondello (1972), and Gibson et al. (1986);
3. 120 UV transitions from Kaufman (1982);
4. 200 transitions from Meißner et al. (1933) and Frerichs (1933);
5. 68 transitions from Jakobsson (1967);
6. 34 two-photon UV transitions from Pratt (1988);
7. Seven two-photon UV transitions from Lai et al. (2020);
8. Six transitions from Alder et al. (1978);
9. Three forbidden transitions from Eriksson (1978);
10. One forbidden transition from Haas et al. (1991);
11. One forbidden far-IR transition from Brown et al. (1994).

For many lines, wavelengths observed by both Meißner et al. (1933) and Frerichs (1933) had been averaged by Kaufman & Martin (1993). These averaged wavelengths appear to have somewhat lower uncertainties compared to the original individual measurements. Thus, we have used those averaged wavelengths of Kaufman & Martin (1993) in our level optimization. Similarly, Kaufman & Martin (1993) had averaged some of the wavelengths measured by both Gibson et al. (1986) and Tondello (1972) or by both Joshi et al. (1987) and Tondello (1972). In all these cases, we have used the wavelengths listed by Kaufman & Martin (1993). Measurement uncertainties were not specified in many of the original publications. A notable exception is the work of Kaufman (1982), where the wavelength uncertainty is specified for each listed line. We have used the method described by Kramida (2013) to evaluate the wavelength measurement uncertainties where they were missing. Where possible, we started with rough estimates provided by the authors. For example, Tondello (1972) described their measurement uncertainties as follows: “The precision is estimated to be about 0.01 Å; however, for considerably broadened or autoionized lines the precision in wavelength could be much smaller.” Nonetheless,

all their wavelengths were given with no more than two decimals after the point (in angstroms), indicating that the given estimate pertains to the systematic uncertainty rather than the total one. Based on comparisons with the Ritz wavelengths obtained from a preliminary level optimization, we estimated that for most wavelengths given with two decimal places after the point the uncertainty is about 0.03 Å, increasing up to 0.1 Å for lines marked as wide, blended, or unresolved. For lines corresponding to transitions from unresolved upper terms, additional information was gleaned from calculations such as those of Kurucz (2004) and Zatsariny & Bartschat (2006), which provided estimates of fine-structure splitting in those terms. Similarly, Meißner et al. (1933) had specified that his measurement accuracy was about ± 0.03 Å for recordings made with a concave grating, but some of his measurements were made with a flat grating with twice greater uncertainties. From comparisons with the Ritz wavelengths, we assessed that most of his measurements below 6800 Å had an uncertainty of 0.03 Å, except for weak and unresolved lines where it was greater, up to 0.07 Å. For wavelengths above 6800 Å, we estimated that the wavelengths reported by Meißner et al. (1933) and Frerichs (1933) have uncertainties of 0.06 Å, while the average wavelengths listed by Kaufman & Martin (1993) with references to those two works are somewhat more accurate, with average uncertainties of about 0.05 Å.

The complete list of transitions included in our level optimization procedure is given in Table 3. There are 869 transitions corresponding to 664 unique observed lines. In addition to wavelengths and their uncertainties for each transition, this table also includes the weight factors used in cases where multiple transitions are assigned to the same observed line. These weights have been estimated from weighted transition probabilities, $g_k A_{ki}$, taken from the compilation of Podobedova et al. (2009), where available, or otherwise from Kurucz (2004) (see Section 3.4). A detailed explanation of the use of these weights in the level optimization is given in Kramida (2011). The relative observed intensities in Table 3 have been reduced to two separate unified scales, one for emission and the other for absorption lines. This reduction is explained further in Section 3.5.

In the sample of Table 3 included in the main text, the lower and upper energy levels of each transition are identified by their energy and J values, and the standard uncertainties of observed and calculated wavelengths are given in parentheses in units of the last decimal figure of the value. In the full machine-readable table, the uncertainties are given in separate columns in the same units as the values; configuration and term labels of the energy levels are included in additional columns. The values of the residual wavenumber differences, $\Delta\sigma_{\text{obs-Ritz}}$, are nonblank only where they are meaningful. For example, if an upper level is defined by a single observed transition, the residual is zero

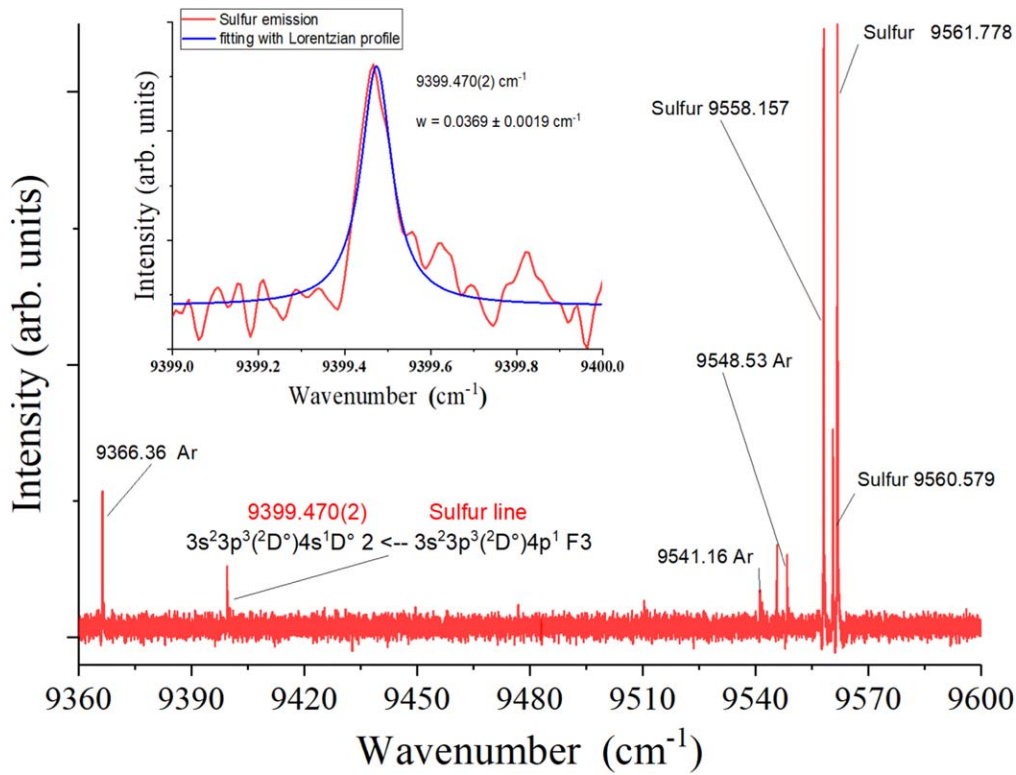


Figure 5. Remeasured lines in the (9300–9600) cm^{-1} range of the S I spectrum.

by definition and thus is left blank. Similarly, for unresolved terms defined by a single observed line encompassing multiple unresolved fine-structure transitions, the residuals for each unresolved transition are close to zero and are not meaningful; thus, they are omitted.

The previously recommended list of S I levels given in the NIST ASD Kramida et al. (2023) was largely based on the observations of Kaufman (1982). The fine structure of the ground configuration (except $3p^4\ ^3P_0$) was derived from the measurements of three forbidden transitions by Eriksson (1978); we have also used these measurements. However, the connection between the ground and excited configurations relied on the numerous lines observed by Kaufman (1982) in the vacuum ultraviolet region. The recent high-precision measurement of several two-photon transitions of the type $3p^4\ ^3P_J\text{--}3p^3(^4S^o)4p\ ^3P_J$ by Lai et al. (2020) has opened a possibility to drastically improve the accuracy of the excited level system. This team made their measurements for a single isotope, ^{32}S . Since all other observations of the S I spectrum were made with natural sulfur samples, it was necessary to reduce their measurements to natural sulfur. In this regard, scarcity of experimental data on isotope shifts in neutral sulfur presented a serious problem.

Lai et al. (2020) measured the $^{32}\text{S}\text{--}^{34}\text{S}$ isotope shift ($\text{IS}_{32\text{--}34} = \text{IS} = 0.0179(4)\ \text{cm}^{-1}$) of one transition, $3p^4\ ^3P_2\text{--}3p^3(^4S^o)4p\ ^3P_2$. No other IS measurements have been published for S I. However, this one measured IS value can be used for all ^{32}S levels measured by Lai et al. (2020), because the IS of all lines of the same multiplet is nearly the same.

Indeed, since the configurations involved in the above transitions contain no s electrons in the valence subshells, the field term in the transition isotope shift is negligible. As for the

specific mass term, its different values for different individual lines of the multiplet are actually due to the dependence of the corresponding diagonal matrix elements on the total angular momentum, J , of the energy levels involved. Such a dependence is, in turn, due to relativistic effects, which have an additional smallness of the order of $(\alpha Z)^2$ where $\alpha \simeq 1/137$ is the fine-structure constant. For example, this smallness is well illustrated both experimentally and numerically for the $2p^54p$ and $2p^53d$ configurations of Ne I by Keller (1973). According to his Table 1, the difference between the isotope shifts for the lines with different J is smaller than $\approx 0.4\ \text{mK} = 0.0004\ \text{cm}^{-1} \ll \text{IS}$. For S I, Veseth (1985) calculated the $\text{IS}(^{34}\text{S}\text{--}^{32}\text{S})$ for the $3p^4\ ^3P_2\text{--}^3P_1$ and $^3P_1\text{--}^3P_0$ fine-structure intervals to be $-0.0005\ \text{cm}^{-1}$ and $-0.0002\ \text{cm}^{-1}$, respectively.

Therefore, for a transition from the $3p^4\ ^3p\text{--}3p^3(^4S)4p\ ^3P$ multiplet in ^{32}S with the wavenumber σ_{32} (and uncertainty $\delta\sigma_{32}$) we can determine its wavenumber in ^{34}S as $\sigma_{34} = \sigma_{32} + \text{IS}$ and its uncertainty as $\delta\sigma_{34} = \sqrt{(\delta\sigma_{32})^2 + (\delta\text{IS})^2 + \delta_J^2}$, where δIS is the uncertainty of the single IS value measured by Lai et al. (2020) and δ_J is the uncertainty of the J -dependent contribution to the transition IS discussed above. For the $3p^4\ ^3P_2\text{--}3p^3(^4S)4p\ ^3P_2$ transition, for which the IS was directly measured by Lai et al. (2020), $\delta_J = 0$. For the other six transitions having only the ^{32}S wavenumbers measured in the latter work, we conservatively assumed $\delta_J = 0.0008\ \text{cm}^{-1}$, twice greater than the above upper limit for Ne I and similarly greater than the calculated IS in the ground term of S I (Veseth 1985).

Since the isotopic composition of natural sulfur samples is heavily dominated by ^{32}S and ^{34}S , the estimated ^{34}S wavenumbers can be used to derive the corresponding

Table 3
Observed Lines of S I used in the Present Level Optimization

λ_{obs}^a	σ_{obs}^a	Intens. ^b	Ch. ^c	σ_{Ritz}^d	$\Delta\sigma_{\text{obs-Ritz}}^e$	$g_k A_{ki}^f$	Acc. ^g	Type ^h	E_i^i	E_k^i	J_i^j	J_k^j	Weight ^k	TP Ref. ^l	Line Ref. ^m	Note ⁿ
928.98(11)	107,645(13)	1000	g, a	107,645(13)					0.0000	107,645	2	0	1		J87	
946.30(10)	105,675(11)		g, a, B	105,673(10)	1				573.59573	106,247	0	1	1		K93, G86, T72	
1125.27(3)	88,867.6(20)			88,867.6(20)				2P	9238.6090	98,106.2	2	0	1		P88	
1323.5153(8)	75,556.36(5)	72000	g	75,556.237(13)	0.12	3.02e+08	C		396.05648	75,952.293	1	2	1	P09, B98	K82	
1323.5220(8)	75,555.98(5)	8200	g	75,555.724(18)		1.02e+08	C		396.05648	75,951.780	1	1	0	P09, B98	K82	X
1541.008939(20)	64,892.5502(8)			64,892.5514(8)	-0.0012			2P	0.0000	64,892.5514	2	2	1		L20	
2168.8851(20)	46,092.18(4)	1900		46,092.166(4)	0.01				9238.6090	55,330.775	2	1	1		K82	
3677.18(3)	27,187.01(22)	46	i	27,187.06(8)	-0.04	2.06e+05	E		52,623.605	79,810.66	2	3	1	ZB06	M33	
5696.63(3)	17,549.37(9)	250	*	17,549.35(11)		6.06e+06	D+		63,446.038	80,995.39	1	1	0.562	ZB06	M33	
5696.63(3)	17,549.37(9)	250	*	17,549.35(12)		4.71e+06	D+		63,446.038	80,995.39	1	2	0.438	ZB06	M33	
6172.77(5)	16,195.70(13)	73		16,195.72(13)	-0.02	1.88e+06	D		64,888.9325	81,084.65	1	1	1	P09, ZB06	K93, F33, M33	
8826.54(6)	11,326.36(8)	52	*	11,326.512(12)	-0.15	5.56e+05	D		67,816.321	79,142.833	1	2	0.664	ZB06	F33	
8826.54(6)	11,326.36(8)	52	*	11,326.51(6)	-0.15	2.78e+05	E		67,816.321	79,142.833	1	1	0.336	ZB06	F33	
9039.27(6)	11,059.80(7)	990		11,059.742(13)	0.06	2.72e+06	D		64,892.5514	75,952.293	2	2	1	P09, ZB06	F33	
9212.851(3)	10,851.425(4)	31000		10,851.422(3)	0.003	1.95e+08	C		52,623.605	63,475.027	2	3	1	P09, ZB06	TW, J67	
10459.402(6)	9558.157(5)	33000		9558.158(3)	0.000	6.54e+07	B+		55,330.775	64,888.9325	1	1	1	P09, Z97	TW, J67	
10636.0260(23)	9399.4327(20)	4200		9399.4330(20)		1.45e+08	C		69,237.872	78,637.305	2	3	1	P09, ZB06	TW, J67	
10821.177(5)	9238.608(4)	100		9238.6090(23)	-0.001	1.06e-01	C	M1	0.0000	9238.6090	2	2	1	P09, F06	E78	
39322.95(9)	2543.044(6)	220		2543.044(4)	0.000	1.02e+07	C		73,920.945	76,463.989	3	2	1	P09, ZB06	TW, H10	
39854.88(14)	2509.103(9)	1600	*	2509.104(6)	-0.001	6.26e+07	A		76,654.762	79,163.866	5	0	0.384	K04	TW	
123518.9(15)	809.593(10)	61		809.593(10)		7.73e+07	A+		80,509.758	81,319.351	0	0	1	K04	TW	
124794(4)	801.319(25)	9		801.325(9)	-0.01	2.03e+06	C+		77,890.518	78,691.843	2	3	1	P09, ZB06	TW	
				752.70(8)		2.01e+06	C+		79,057.965	79,810.66	2	3	0	P09, ZB06		
252450(20)	396.12(3)			396.0565(7)	0.06	4.20e-03	B	M1	0.0000	396.05648	2	1	1	P09, F06	H91	
563255.7(3)	177.53925(9)			177.53925(9)	0.00000	3.02e-04	B	M1	396.05648	573.59573	1	0	1	P09, F06	B94	

Notes.

^a Observed wavelength [\AA] and wavenumber [cm^{-1}] with their standard uncertainties given in parentheses in units of the last digit of the value. For wavenumbers between 5000 and 50,000 cm^{-1} , the wavelength is given in standard air; otherwise, the wavelength is in vacuum. Conversion between air and vacuum was made with the five-parameter formula from Peck & Reeder (1972).

^b Intensity on a uniform scale in arbitrary units proportional to energy flux under the line contour (see text). For emission and absorption lines, the scales are different. For the three forbidden transitions observed by Eriksson (1978), the intensities are quoted from the above reference.

^c Observed line character: *—intensity is shared by two or more transitions; a—line observed in absorption; B—line is very broad due to autoionization of the upper level; bl—blended line; g—transition involving the ground term; i—identification is uncertain; w—wide line.

^d Ritz wavenumber [cm^{-1}] and its uncertainty.

^e Difference between the observed and Ritz wavenumbers [cm^{-1}]. Only meaningful values are nonblank (see text).

^f Weighted transition probability [s^{-1}] in standard exponential notation (e.g., “3.02e+08” means “ 3.02×10^{08} ”). g_k is the statistical weight of the upper level; A_{ki} is the probability of spontaneous radiative decay from upper level k to lower level i .

^g Accuracy of $g_k A_{ki}$; see <https://physics.nist.gov/PhysRefData/ASD/Html/lineshelp.html#OUTACC> for explanation of the code.

^h Transition type: blank—electric dipole (E1); M1—magnetic dipole; E2—electric quadrupole; 2P—two-photon transition.

ⁱ Lower and upper energy levels [cm^{-1}].

^j Total angular momenta of the lower and upper levels.

^k Weight of transition in the level optimization (see text).

^l References to the sources of transition probabilities: B94—Beideck et al. (1994); B96—Biémont et al. (1996); B98—Biémont et al. (1998); F06—Froese Fischer et al. (2006); K04—Kurucz (2004); M68—Müller (1968); P09—Podobedova et al. (2009); W69—Wiese et al. (1969); Z97—Zerne et al. (1997); ZB06—Zatsarinny & Bartschat (2006).

^m References to the sources of observed wavelengths, intensities, and classifications: A78—Alder et al. (1978); B94—Brown et al. (1994); E78—Eriksson (1978); F33—Frerichs (1933); G86—Gibson et al. (1986); H91—Haas et al. (1991); H10—Hase et al. (2010); J67—Jakobsson (1967); J87—Joshi et al. (1987); K82—Kaufman (1982); K93—Kaufman & Martin (1993); L20—Lai et al. (2020); M33—Meißner et al. (1933); P88—Pratt (1988); SJ84—Sarma & Joshi (1984); T72—Tondello (1972); TW—this work. If multiple references are given, the first one is to the source of the given observed wavelength.

ⁿ Note: I—observed intensity is much greater than predicted by an LTE model; X—this transition was excluded from the level optimization.

(This table is available in its entirety in machine-readable form in the [online article](#).)

wavenumbers of the natural isotope mixture:

$$\sigma_{\text{nat}} = \frac{\sum c_m \sigma_m}{\sum c_m}, \quad (3)$$

where c_m is the abundance of isotope m and σ_m is the corresponding wavenumber.

The latest critical evaluation of isotopic compositions of the elements was made in 2013 by the International Union of Pure and Applied Chemistry (Meija et al. 2016). Their report provides the lower and upper boundaries of isotope abundances observed in natural samples. Taking the arithmetic mean of these boundaries as an estimate of the average abundance, c_m , and half the interval between them as uncertainty, δc_m , we obtain the following data: $c_{32} = 0.9485(44)$, $c_{33} = 0.00763(34)$, $c_{34} = 0.0437(41)$, and $c_{36} = 0.000158(29)$. The uncertainty of σ_{nat} in Equation (3) can be derived by using standard statistical error propagation formulae, e.g., by adding partial uncertainties in quadrature:

$$\delta \sigma_{\text{nat}} = [(\Delta \sigma_{\text{nat}}^{(\sigma)})^2 + (\Delta \sigma_{\text{nat}}^{(c)})^2]^{1/2}, \quad (4)$$

$$(\Delta \sigma_{\text{nat}}^{(\sigma)})^2 = \frac{\sum c_m^2 \delta \sigma_m^2}{(\sum c_m)^2} \quad (5)$$

$$(\Delta \sigma_{\text{nat}}^{(c)})^2 = \frac{\sum [(\sigma_m - \sigma_{\text{nat}}) \delta c_m]^2}{(\sum c_m)^2}. \quad (6)$$

In these equations, $\Delta \sigma_{\text{nat}}^{(\sigma)}$ and $\Delta \sigma_{\text{nat}}^{(c)}$ are the partial uncertainties arising from the terms with σ_m and c_m in Equation (3), respectively.

Since we do not have data for σ_{33} and σ_{36} , we can only make some rough estimates for them.

The total isotope shift of a transition wavenumber is a sum of two major parts, the mass shift and the field shift (see, e.g., Aufmuth et al. 1987). It is well known that the field shift is very small in elements lighter than calcium. For example, as calculated by Veseth (1985) for Ar II, the contribution of field shift to the total IS(^{40}Ar – ^{36}Ar) of the fine-structure transition between the levels of the ground term $3p^5\ ^2P$ is less than 2%. Thus, we have assumed that the IS in all transitions of interest in S I is due to the mass shift only, which is proportional to the mass factor $\frac{A' - A}{AA'}$, where A and A' are nuclear masses of the two isotopes (Aufmuth et al. 1987). To estimate the unknown wavenumbers in ^{33}S and ^{36}S , we have simply scaled the known IS(^{34}S – ^{32}S) to these two isotopes with the use of nuclear masses derived from atomic masses given in the latest atomic mass evaluation by Wang et al. (2021). We have assigned generous 100% uncertainties to these values, i.e., assumed the uncertainties of the same size as the values.

Using the wavenumbers of all transitions observed by Lai et al. (2020) in ^{32}S estimated for all other isotopes as described above, we have applied Equations (3)–(6) to derive the corresponding wavenumbers and their uncertainties for natural sulfur samples. These values are included in Table 3. The contributions of ^{33}S and ^{36}S to these final values turned out to be negligibly small, so their large uncertainties have no influence on the present results.

We have also included the $3p^4\ ^3P_1$ – 3P_0 separation from far-IR magnetic resonance laser measurements by Brown et al. (1994). We adopted this result as corresponding to natural sulfur, although we cannot exclude that the way they observed the signal from a natural sulfur sample may have led to a shift

of the resonance position that is not proportional to isotope abundances.

Including the data from Lai et al. (2020) and Brown et al. (1994) had a significant effect on the optimized level values. When we made a level optimization without accounting for these data, the resulting level values were close to those reported by Martin et al. (1990). However, when we included them, the excited levels below the first ionization limit have shifted down by $-0.035\ \text{cm}^{-1}$ on average, including the $3p^4\ ^3P_0$ level, which decreased by $0.044\ \text{cm}^{-1}$. This shift seemed to be too large given that Martin et al. (1990) had specified the uncertainties of their $3p^4\ ^3P_0$ level value as $\pm 0.016\ \text{cm}^{-1}$ and uncertainties of the higher excited levels as about $\pm 0.02\ \text{cm}^{-1}$. However, when we have utilized the option available in LOPT for tracing the contributions of systematic errors in wavelength measurements (see Kramida 2011), which showed that the total uncertainty of the connection of excited levels to the ground term in measurements of Kaufman (1982) was about $0.03\ \text{cm}^{-1}$. Thus, Kaufman's measurements are, in fact, statistically compatible with the high-precision data derived from Lai et al. (2020) and Brown et al. (1994).

As mentioned above, the average shift of the newly optimized levels from those of Martin et al. (1990) is $-0.035\ \text{cm}^{-1}$. However, it is an unweighted mean. A more meaningful parameter is a weighted mean with weights inversely proportional to squared uncertainties. This weighted average shift turns out to be much smaller, only $-0.013(2)\ \text{cm}^{-1}$. Its origin can be traced to a small systematic shift in the measurements of Kaufman (1982), which is illustrated in Figure 6. We should note that a few lines having very large error bars have been excluded from this figure, along with the strongly deviating line at $1323.5153\ \text{\AA}$, which will be discussed further below. The dotted line representing an unweighted linear fit to the data points has an offset of $0.010\ \text{cm}^{-1}$ from zero and a negligibly small slope. This offset is entirely compatible with the weighted average shift in the optimized levels. It is much smaller than the average measurement uncertainty of Kaufman (1982), which is $0.05\ \text{cm}^{-1}$ for his 46 UV lines having uncertainties of $0.001\ \text{\AA}$ or smaller.

The list of our optimized energy levels of S I is presented in Table 4. There are 114 even-parity and 263 odd-parity levels. Along with our new results, this table also includes the previous energy-level values from the NIST ASD (Kramida et al. 2023) and the differences between the new and old values, where they are meaningful from the point of view of statistics. For two levels discussed further below, the energies have been revised. For these levels, a direct comparison is not statistically meaningful. It is also not meaningful for levels having uncertainties greater than about $0.25\ \text{cm}^{-1}$. Most of these levels are located above the ionization threshold and have not changed in our level optimization. The rms value of the reduced difference between the two data sets (i.e., the difference divided by its uncertainty), accounting only for the nonblank differences in Table 4, is 1.09, indicating a good agreement.

On the other hand, by comparing the uncertainties of the new and old energy-level values in Table 4, one can see that for levels below $83,000\ \text{cm}^{-1}$ the uncertainties have been reduced by a factor of five on average. For 17 levels, this reduction is by a factor of 10 or greater. This allows us to say that, while

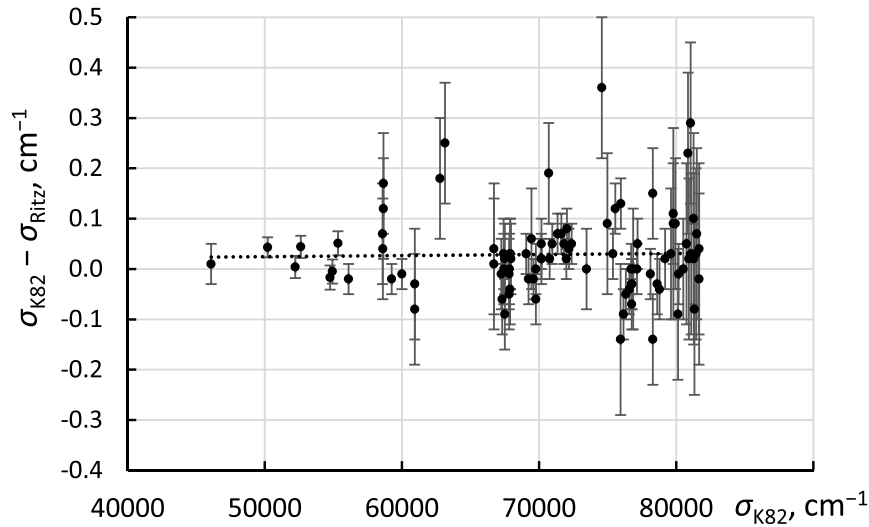


Figure 6. Comparison of UV transition wavenumbers observed by Kaufman (1982) (σ_{K82}) with the Ritz values (σ_{Ritz}) calculated from the newly optimized energy levels. The error bars are those of Kaufman (1982). The dotted line is an unweighted linear fit to the data points.

agreeing with previously available data, our new set of energy levels is significantly more accurate.

We note that many terms of SI have a very small fine structure that could not be resolved in observed spectral lines. Many of such unresolved terms are defined by a single observed spectral line. It does not make sense to derive several different fine-structure energy values from a single observed line. In such cases we have fixed the fine-structure intervals at zero by introducing in the level optimization the so-called virtual lines with zero wavenumbers for transitions between the fine-structure components (see Kramida 2011). A similar fixing of the fine structure at zero was made for the terms defined by a few observed lines whose precision was insufficient to derive the fine structure with any reasonable accuracy. Examples of such too-poorly resolved terms are $3p^3(^4S^o)nf\ ^5F$ and 3F ($n = 5-8$). For such unresolved levels, Table 4 gives the same energy value for all fine-structure components, but the uncertainties may differ significantly because they are estimated from the weights of the corresponding transitions, which are in turn defined by calculated relative intensities. Thus, the fine-structure level contributing the strongest transition to an observed blended line receives the smallest uncertainty.

Internal consistency of the data (spectral lines collected from all the sources above) is characterized by the values of reduced residuals $R_i = (\sigma_{obs,i} - \sigma_{calc,i})/u_i$, where $\sigma_{obs,i}$ and u_i are the observed wavenumber and its uncertainty for the line i , and $\sigma_{calc,i}$ is the Ritz wavenumber for this line, which equals the difference between the upper and lower energy levels of this transition. For the measurements to be consistent with the given identifications, the rms value of R_i must be close to or smaller than 1. In our level optimization, it was about 0.8. To check if all identifications and measurements are correct, the distribution of the R_i values should be close to the normal statistical distribution. So we draw a normal probability plot (see Figure 7) where the reduced residuals R_i are plotted against the values of corresponding normal order statistic medians, $G(U_i)$ where G is the percent point function of the uniform order statistic medians, U_i ; see details in the NIST Engineering Statistics Handbook (Heckert et al. 2012, Section 1.3.3.21). Figure 7 includes only those R_i values that were deemed “meaningful” as defined in Section 3.2. Additionally, blended

transitions having a small weight in the level optimization (<0.1) have been omitted from this plot because their residuals are not statistically meaningful. For a good, normally distributed set of measurements, the points in this plot must be grouped around a straight line with a unit slope passing through the origin (0, 0).

For our full set of transitions, the actual value of the slope is 0.84, the vertical offset from the origin is 0.035, and the distribution of the points is close enough to a straight line.

We note that one line reported by Kaufman (1982) at 1323.5220(8) Å strongly deviated from our newly determined Ritz wavelength. The reduced residual value for this line is 5.1, meaning that its observed wavelength disagrees with the more accurate Ritz value, 1323.5265(3) Å by more than five times the specified measurement uncertainty. This line was excluded from our level optimization, as well as from the plot in Figure 7. The cause of this deviation is unclear. We note that this line is only 7 mÅ away from the 9 times stronger line observed by Kaufman (1982) at 1323.5153(8) Å, so it could not be possible to completely resolve it in Kaufman’s experiment. It seems likely that the small uncertainty given by Kaufman for this weaker line was just a technical error in his paper.

Three levels in Table 4 have a note “E”, meaning that an error in their energy has been corrected. One of them, $3p^3(^2D^o)4p\ ^1F_3$, has already been discussed above in Section 3.1. For this level, the error in the NIST ASD Kramida et al. (2023) stemmed from an error in the line list of Jakobsson (1967). Another corrected level is $3p^3(^4S^o)6d\ ^5D_0$. For this level, the energy value specified in the NIST ASD Kramida et al. (2023) was a result of an unknown technical error. This level is corrected here by including it in the unresolved $3p^3(^4S^o)6d\ ^5D_{0,1,2}$ group based on calculations of Kurucz (2004) and Zatsarinny & Bartschat (2006).

The third level with an “E” note is $3p^3(^4S)7p\ ^5P_3$. Its value in the NIST ASD (and in Martin et al. 1990), 79,785.52 cm⁻¹, is probably incorrect. The compilation of Kaufman & Martin (1993) does not contain any observed transitions from this level. It was first identified by Meißner et al. (1933) based on a single line observed at 3677.18 Å (in air), placing it at a different energy, i.e., 79,810.68 cm⁻¹. There is another combining line observed in the same work but given as

Table 4
Optimized Levels of S I

Configuration	Term	J	E_{TW}^{a} (cm^{-1})	u_{TW}^{b} (cm^{-1})	$E_{\text{prev}}^{\text{c}}$ (cm^{-1})	$u_{\text{prev}}^{\text{d}}$ (cm^{-1})	$\Delta E_{\text{TW-prev}}^{\text{e}}$ (cm^{-1})	$N_{\text{lines}}^{\text{f}}$	Note ^g
$3s^23p^4$	3P	2	0.0000	0.0000	0.000	0.000		177	
$3s^23p^4$	3P	1	396.05648	0.00069	396.055	0.005	0.001	72	
$3s^23p^4$	3P	0	573.59573	0.00068	573.640	0.016	-0.044	38	
$3s^23p^4$	1D	2	9238.6090	0.0023	9238.609	0.005	0.000	47	
$3s^23p^4$	1S	0	22,179.9542	0.0022	22,179.954	0.005	0.000	7	
$3s^23p^3(^4S^{\circ})4s$	$^5S^{\circ}$	2	52,623.605	0.004	52,623.640	0.022	-0.035	13	
$3s^23p^3(^4S^{\circ})4s$	$^3S^{\circ}$	1	55,330.775	0.003	55,330.811	0.022	-0.036	14	
$3s^23p^3(^4S^{\circ})4p$	5P	1	63,446.038	0.004	63,446.065	0.022	-0.027	22	
$3s^23p^3(^4S^{\circ})4p$	5P	2	63,457.1166	0.0039	63,457.142	0.022	-0.025	20	
$3s^23p^3(^4S^{\circ})4p$	5P	3	63,475.027	0.004	63,475.051	0.022	-0.024	17	
$3s^23p^3(^4S^{\circ})4p$	3P	1	64,888.9325	0.0011	64,888.964	0.022	-0.031	31	
$3s^23p^3(^4S^{\circ})4p$	3P	0	64,891.3536	0.0011	64,891.386	0.022	-0.032	15	
$3s^23p^3(^4S^{\circ})4p$	3P	2	64,892.5514	0.0011	64,892.582	0.022	-0.031	28	
$3s^23p^3(^4S^{\circ})5g$			79,163.866	0.005				9	N
$3s^23p^3(^4S^{\circ})7p$	5P	3	79,810.66	0.08	79,785.52	0.08		2	EQ
$3s^23p^3(^4S^{\circ})6g$			80,507.180	0.005				13	N
$3s^23p^3(^4S^{\circ})6h$			80,509.758	0.007				1	N
$3s^23p^3(^4S^{\circ})7g$			81,317.143	0.006				15	N
$3s^23p^3(^4S^{\circ})7h$			81,318.833	0.007				2	N
$3s^23p^3(^4S^{\circ})7i$			81,319.351	0.012				1	N
$3s^23p^3(^2D^{\circ})3d$	$^3F^{\circ}$	3	82,604.40	0.08	82,604.41	0.08	-0.01	1	R
$3s^23p^3(^2D^{\circ})3d$	$^1D^{\circ}$	2	85,614	3	85,614	3		2	D
$3s^23p^3(^2P^{\circ})16d$	$^3PD^{\circ}$		107,645	13	107,645	10		1	

Notes.^a Level value optimized in this work.^b Uncertainty is given for the separation from the ground level.^c The level value previously reported in the NIST ASD (Kramida et al. 2023; Kaufman & Martin 1993; Martin et al. 1990.)^d Uncertainty of the previous level value as inferred from the explanatory text in Martin et al. (1990).^e The difference is nonblank only where it is meaningful for the purpose of comparison. It is left blank for all new and revised levels, as well as for levels with large uncertainty, for which the change is negligible.^f Number of transitions participating in the level determination.^g Notes: —unobserved level (the energy was derived by Martin et al. (1990) from series formulae); a—this level may have a significant autoionization rate (quoted from Martin et al. (1990)); u—unresolved level; C—confirmed identification (previous question marks removed; see text); D—designation of this level is questionable (see text); E—the previous erroneous energy value has been corrected (see text); N—new identification; R—designation of this level has been revised (see text); Q—questionable level.(This table is available in its entirety in machine-readable form in the [online article](#).)

unidentified, at 8377.79 Å (in air), corresponding to the $3p^3(^4S^{\circ})3d\ ^5D_4^{\circ}-3p^3(^4S^{\circ})7p\ ^5P_3$ transition. Martin et al. (1990) must have based their value of $3p^3(^4S^{\circ})7p\ ^5P_3$ on the neighboring line from Meißner et al. (1933) (at 8395.63 Å), which they assigned to that transition, $3d\ ^5D_4^{\circ}-7p\ ^5P_3$. It yields the level value 79,785.32 cm^{-1} , only slightly different from the one listed in Martin et al. (1990). Since the combination of two lines observed by Meißner et al. (1933) supports his identification of the $3p^3(^4S^{\circ})7p\ ^5P_3$ level, we have tentatively adopted his assignment and corrected the energy accordingly. However, both these lines appear to be a few times stronger than predicted from transition probabilities calculated by Zatsarinny & Bartschat (2006). These authors have also predicted several potentially observable transitions from $3p^3(^4S^{\circ})7p\ ^5P_3$ that are located in the IR range covered by our observations. Their predicted intensities are rather small, close to the level of noise in our observed spectra. We could not find any of these transitions in our spectrograms. Thus, this level is additionally marked as questionable in Table 3.

Two levels with a note “J” in Table 4 have no observed transitions. These levels are $3p^3(^4S^{\circ})10d\ ^5D_4^{\circ}$ and $3p^3(^2D^{\circ}_{3/2})15f$. Their values are quoted from Martin et al. (1990), where they were derived by interpolation along the

corresponding Rydberg series. The latter level represents a degenerate subconfiguration, similar to all other autoionizing Rydberg levels observed by Pratt (1988) with two-photon spectroscopy.

The level $3p^3(^2D^{\circ})3d\ ^3F_3^{\circ}$ at 82,604.40 cm^{-1} has a note “R”, meaning that its designation has been revised. This level was previously designated as $^1F_3^{\circ}$ (Kramida et al. 2023; Martin et al. 1990). However, several calculations indicate that it should be $^3F_3^{\circ}$ (see, e.g., Zatsarinny & Bartschat 2006; Kurucz 2004). The $3p^3(^2D^{\circ})3d\ ^1F_3^{\circ}$ level is now unidentified, which is rather strange, as according to Kurucz’s calculation (Kurucz 2004), the lines originating from it should be much stronger than those from $^3F_3^{\circ}$. The same calculation of Kurucz predicts the $3p^3(^2D^{\circ})3d\ ^1F_3^{\circ}$ level close to the position of the level observed at 85,614 cm^{-1} , which is currently identified as $3p^3(^2D^{\circ})3d\ ^1D_2^{\circ}$. Both observed lines assigned to this level have lower levels with $J=2$, which makes it possible that it is actually not $^1D_2^{\circ}$ but the missing $^1F_3^{\circ}$ level. Hence, we have marked the $3p^3(^2D^{\circ})3d\ ^1D_2^{\circ}$ level as having a questionable designation.

We have removed the question marks from two levels having those marks in Martin et al. (1990), $3p^3(^2D^{\circ})4d\ ^3P_0^{\circ}$ and $3p^3(^2P^{\circ})5s\ ^3P_0^{\circ}$. Each of these levels is determined by a single

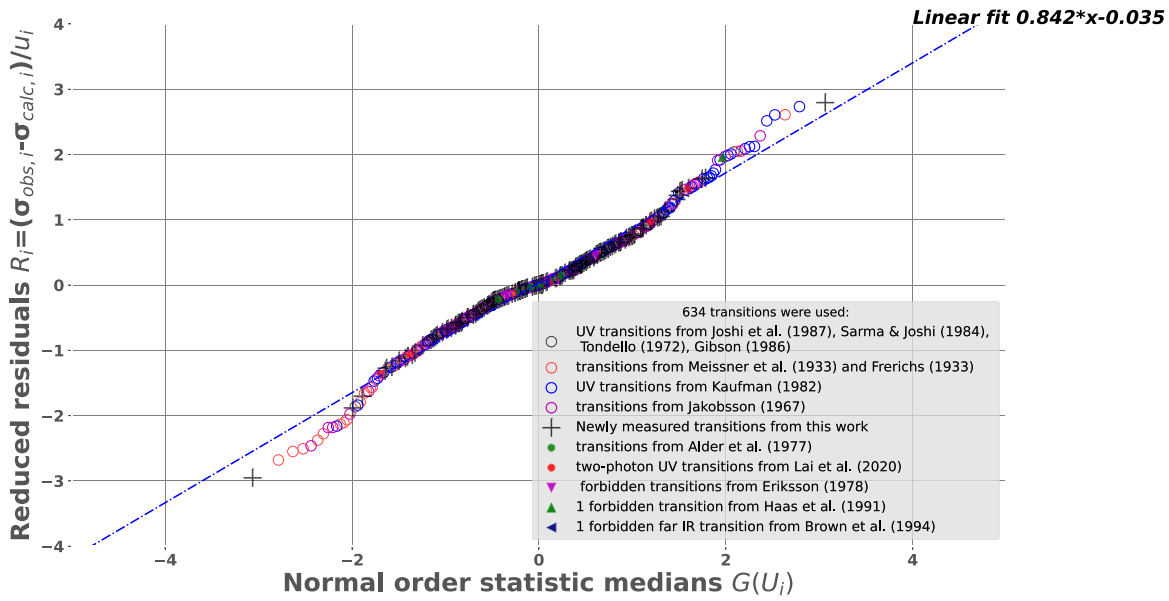


Figure 7. The normal probability plot for the R_i values (see the text).

line. Both of these lines (at 1098.02 Å and 1055.03 Å, respectively) were observed in absorption by Joshi et al. (1987); the first line was also observed by Tondello (1972). Their intensities reported by Joshi et al. (1987) are in fair agreement with calculations of Kurucz (2004). We searched for possible alternative identifications in the list of transitions predicted by Kurucz (2004). This list includes transitions from previously unidentified energy levels. The uncertainty in their calculated energies can be estimated from the standard deviation of Kurucz’s calculated levels from known experimental ones. For odd-parity levels, it is about 35 cm^{-1} . This corresponds to about 0.4 Å uncertainty in the predicted wavelengths around 1100 Å . We searched for strong predicted transitions from previously unidentified levels within $\pm 1.5 \text{ Å}$ from these two observed wavelengths and did not find any. Thus, the assignments given in Table 3 (quoted from Kaufman & Martin 1993) appear to be the only possible ones.

One level listed as questionable by Martin et al. (1990), $3p^3(^2D^o)6s \ ^1D_2^o$, remains unconfirmed because there is no information about the intensity of the absorption line that solely determines this level in the study of Tondello (1972).

The six levels included in Table 4 with a note “N” are the ones newly found in our IR FTS spectra. They represent centers of gravity of quasi-degenerate configurations $3p^3(^4S^o)ng$ ($n = 5, 6, 7$), $3p^3(^4S^o)nh$ ($n = 6, 7$), and $3p^3(^4S^o)7i$. All of them have been determined with small uncertainties ranging from 0.005 to 0.012 cm^{-1} . For each of the ng configurations, we have observed two distinct lines down to the quintet and triplet terms of $3p^3(^4S^o)4f$, and for $7g$, also two lines to $3p^3(^4S^o)5f$. Nevertheless, we were not able to derive any fine structure in them. According to our calculations made with Cowan’s codes (Cowan 1981; Kramida 2021), all the $3p^3(^4S^o)ng$, nh , and ni subconfigurations are almost pure in the $LSjj$ coupling scheme (with purity ranging from 95% to 100%), and their widths are very small, $3p^3(^4S^o)5g$ being the widest with a width of about 0.033 cm^{-1} . Kurucz’s calculation (Kurucz 2004) gave a significantly smaller width of 0.008 cm^{-1} for this configuration, from which we concluded that theoretical fine-structure splittings are insufficiently

accurate to attempt a derivation of the fine structure from our observed lines.

3.3. Ionization Energy of S I

The energies of the $5g$, $6g$, $7g$, $6h$, $7h$, and $7i$ levels listed in Table 4 can be used to improve the ionization energy (IE) of S I. It can be derived by fitting a polarization formula from Edlén (1964) by running the POLAR code (Kramida 2013) with the values and their uncertainties from Table 4. The polarization formula mentioned above is an approximation for the energy of nonpenetrating (i.e., high- l) Rydberg levels. This approximation is more elaborated than the Rydberg formula (2), and includes the dependence of energies (E_{nl}) on dipole (α_d) and quadrupole (α_q) polarizabilities of the atomic core. As a result of nonlinear fitting of the experimental energies of high- l Rydberg levels to the polarization formula, one obtains the α_d , α_q and IE values. The uncertainties of these parameters are combinations in quadrature of the fitting uncertainty and the uncertainty arising from the level uncertainties. With this method, we obtained $\text{IE} = 83,559.170(11) \text{ cm}^{-1}$, which is more accurate than the currently recommended value, $83,559.1(10) \text{ cm}^{-1}$ (Kramida et al. 2023; Martin et al. 1990), by 2 orders of magnitude. It is also worth noting that the dipole polarizability, $\alpha_d = 10.564(17)$ atomic units (a.u.) resulting from our fitting, is close to the value $\alpha_d = 10.24$ a.u. obtained by variational calculations with configuration interaction expansion (Hibbert 1980). Our fitted value of $\alpha_q = -1.8(27)$ a.u. is statistically consistent with zero.

3.4. Transition Probabilities

Transition probabilities (TPs) play an important role in determination of energy levels. Namely, when there are unresolved blends of several transitions (and there are numerous such blends in S I), their contributions to the measured central wavelength must be weighted according to their predicted intensities. When the upper energy levels of the blended transitions ($i \rightarrow k$) are close to each other (and this is the case for most of S I blends), the emitted intensities (in optically thin plasmas in local thermodynamic equilibrium) are proportional to weighted TP ($g_k A_{ki}$). The LOPT code (Kramida 2011) allows for

the use of such weighting. The NIST ASD database presents TP data critically compiled by Podobedova et al. (2009). Unfortunately, this compilation does not cover all blends present in the spectrum, so it was complemented from a rather good calculation of Robert L. Kurucz (2004), the results of which are available in the `/atoms/1600/` directory of his Atoms database. The $\log(g_i f_{ik})$ -values for transitions between all experimentally known levels can be found in his `gf1600.pos` file, while transitions from all levels below the ionization limit, including the $(^4S^o)ng$, nh , and ni levels, can be found in the `gf1600.low` file.

To evaluate the accuracy of Kurucz's calculated TPs, we used the method outlined by Kramida (2013). Namely, we compared Kurucz's TP values with the benchmark data critically compiled by Podobedova et al. (2009). From the distribution of comparison statistics, we have derived an estimate of uncertainty as a function of line strength. It turned out that for a few strongest transitions with line strength $S > 1000$ a.u. Kurucz's results are fairly accurate, deviating from the benchmark values by less than 2%. With decreasing S , the accuracy of his results quickly degrades, but remains acceptable ($\leq 50\%$) for $S > 20$ a.u. Even for rather weak transitions with S as small as 10^{-4} a.u., Kurucz's TP values are still within 1 order of magnitude from the benchmark data.

We noticed that many transitions calculated by Kurucz (2004) were also calculated by Zatsarinny & Bartschat (2006) (hereafter, referred to as **ZB06**) but were not included in the compilation of Podobedova et al. (2009) despite, as noted in that compilation, the relativistic B-spline R-matrix (BSR) calculation of **ZB06** being the most accurate available. Thus, we made an effort to evaluate the accuracy of this calculation as well. Since a very large fraction of the data included in the compilation of Podobedova et al. (2009) were taken from **ZB06**, it was not possible to use the same method of evaluation as for Kurucz's data. However, **ZB06** have provided in their supplementary data table the magnitude of discrepancy between the length and velocity forms of their calculated line strength. We have used this accuracy indicator in the same statistical framework outlined by Kramida (2013) to derive the uncertainties of the length-form line strengths of **ZB06** as a function of S . This showed that, indeed, the results of **ZB06** are in most cases superior to those of Kurucz (2004). It also indicated that the uncertainty estimates assigned to the **ZB06** data by Podobedova et al. (2009) are exaggerated in many cases and probably need to be revised. However, a comprehensive re-evaluation of all published TP data for S I is outside the scope of the present work, so the accuracy codes assigned by Podobedova et al. (2009) are left unchanged in our Table 3. We have restricted ourselves to providing only the results of our evaluation for transitions not included in Podobedova et al. (2009).

In addition to 358 TP values quoted from Podobedova et al. (2009), Table 3 includes 98 newly evaluated TP values from **ZB06** and 43 from Kurucz (2004). Most of the latter values correspond to transitions that were not considered in **ZB06**.

For about half of all transitions participating in multiply classified observed lines, the TP values were available from Podobedova et al. (2009). We utilized them in the calculation of line weights. Among the remaining 460 blended transitions, only a small fraction had data in **ZB06**, but all of them were included in Kurucz (2004). Thus, we have used Kurucz's

results to calculate the weights for transitions not included in Podobedova et al. (2009). However, we have used all critically evaluated TP data of Table 3 in the reduction of observed intensities described in the Section 3.5.

The TP values for transitions from degenerate configurations $3p^3(^4S^o)nl$ ($n=5, 6, 7, l=g, h, i$) included in Table 3 correspond to the sums of fine-structure line strengths derived from the $\log(g_i f_{ik})$ values given by Kurucz (2004). Although Kurucz gave only *LS*-coupling designations for all calculated levels, calculation of total line strengths from the ng configurations down to the quintet and triplet levels of $3p^3(^4S^o)nf$, as well as those for the $ng-nh$ and $nh-ni$ transitions, was fairly straightforward. We note that these line strengths are in excellent agreement with our Cowan-code calculations, which were made specifically to verify Kurucz's results, as well as with our QDT calculations mentioned in Section 3.1.

To facilitate future research aimed at confirmation of the presently questionable identification of the $3p^3(^4S^o)7p^5P_3$ level, we included in Table 3 the calculated $g_k A_{ki}$ values from Zatsarinny & Bartschat (2006) for a few strongest predicted transitions from this level.

3.5. Reduction of Observed Line Intensities

As one can see in our Table 2, the scales of our observed relative intensities are vastly different in different spectral regions. Previous researchers (Frerichs 1933; Meißner et al. 1933; Jakobsson 1967; Kaufman 1982) have also used intensity scales differing not only between the various studies but also between different spectral regions covered in each study. To reduce all observed intensities to a common uniform scale, we have used the method best described by Kramida et al. (2022) employing a simple model of level populations assuming local thermodynamic equilibrium (LTE) in absence of self-absorption and using the critically compiled transition probabilities described in Section 3.4.

The method we used for intensity reduction involves two main procedures: derivation of the Boltzmann plot used to derive the effective excitation temperature and derivation of the instrumental response correction as a function of wavelength (Kramida et al. 2022). Response correction functions are built by plotting the logarithmic ratio $\ln(I_{\text{calc}}/I_{\text{obs}})$ (where I_{calc} and I_{obs} are the calculated and observed intensity, respectively) against wavelength and fitting these scatter plots with polynomials. The degree of the polynomials used in the present work was between 0 and 3. In our measurements, each of the six spectral regions separated by thick horizontal lines in Table 2 represents a separate experiment with different detectors, bandpass filters, and plasma conditions. The effective temperatures derived from Boltzmann plots were between 0.3 eV and 0.4 eV in most regions, except for 0.7 eV in the region from 7000 to 11,000 cm^{-1} (9200 Å to 14000 Å) and 0.08 eV in the region from 5300 to 5600 cm^{-1} (18100 Å to 18700 Å).

The intensities reported by Frerichs (1933) and by Meißner et al. (1933) were found to be on a logarithmic scale with a base of square root of 2 in Frerichs (1933) and about 1.25 in Meißner et al. (1933). Reduction of these intensities was made after conversion of the reported values to a linear scale. Frerichs had used five different types of photographic plates in his wide spectral range. The ranges using different plates displayed notably different behaviors of spectral response, so the response correction functions were built separately for each

of the five corresponding spectral regions. However, due to lack of information about excitation conditions, we assumed that the effective temperature was the same in all exposures (it turned out to be about 0.6 eV). The fairly smooth behavior of the spectral response functions indicated that this assumption provides a good approximation. Meißner et al. (1933) had also used a few different plate types in his observations, but the spectral response function built from his observed intensities behaved sufficiently smoothly across the entire spectral range of his study. The effective temperature derived from Meißner's observed intensities is about 0.5 eV.

Jakobsson (1967) reported three sets of observations. The most extensive set was produced with photoelectric measurements of intensities. For this set, the effective temperature resulting from our modeling is 0.5 eV. The much smaller data sets recorded with photographic plates and with a PbS detector contained lines with a very narrow range of excitation energies for upper levels of observed transitions. This precluded derivation of excitation temperature from Boltzmann plots, so we have assumed the same temperature as for his photoelectric recordings.

Observations of Kaufman (1982) in the VUV region displayed sharp variations of the spectral response. Despite the absence of any information about the photographic plates used in his work, it was possible to divide Kaufman's observations into six separate regions of a size varying between 60 Å and 340 Å. The shortest regions were those adjacent to the wavelength for which his grating was blazed (1200 Å). We assumed the same excitation conditions (i.e., temperature) for all six regions. The effective temperature was found to be 0.7 eV for Kaufman's observations. Several intensity values reported by Kaufman cannot be explained by our rough model. Most of them correspond to transitions from the three levels of the $3s3p^5$ configuration down to the levels of the ground configuration, $3s^23p^4$. These transitions are extremely difficult to calculate because of the strong interaction between the $3s3p^5$ $^3P^o$ term and the $3s^23p^3(^2D^o)nd$ $^3P^o$ series. Various calculations, e.g., by Zatsarinny & Bartschat (2006), Kurucz (2004), and our Cowan-code calculations produced g_kA_{ki} values differing by several orders of magnitude for these transitions. However, six of them were measured by Müller (1968) and are included in the NIST ASD (Kramida et al. 2023) with an estimated uncertainty of less than 50%. The observed intensities reported by Kaufman (1982) for these transitions are greater than the calculated ones by a factor between 600 and 2000. Aside from a possibility of the measurements of Müller (1968) or intensity values of Kaufman (1982) being grossly incorrect, the only plausible explanation we can come up with is that the $3s3p^5$ levels were greatly overpopulated in the microwave discharge used by Kaufman and cannot be described by our simplistic LTE model. Thus, these lines were excluded from our modeling of Kaufman's intensities. The lines for which the observed intensity is much greater than predicted by an LTE model are marked with a note "I" in Table 3.

Since the observations having an effective temperature of 0.7 eV (Kaufman's and ours) contained the largest number of observed lines, Kaufman's intensity scale (multiplied by 100 and corrected for variations of spectral response) was chosen as the base of our unified emission intensity scale. By using the simple method explained in Kramida et al. (2022), we reduced all observed relative intensities to this scale. For lines observed

in several studies, we adopted a logarithmic average of all intensities reduced to the base scale. For about one-third of all lines observed in emission, relative intensities were reported in two studies, and for several lines there were three or four observations. Despite the fact that we have included in our modeling only those g_kA_{ki} values that were deemed to be accurate within a factor of up to 5, the largest disagreement between the multiple available reduced intensity values is only a factor of 2.5, and the average standard deviation between them is 25%.

For the three forbidden lines observed in emission by Eriksson (1978), we have retained his originally reported values. Intensities of such forbidden lines strongly depend on plasma density and temperature, so these values have little practical meaning.

In absorption spectroscopy studies of S I, observed intensity values were reported only by Joshi et al. (1987) and Sarma & Joshi (1984). Among the lines included in Table 3 with references to these two studies, only two have not been reported by Joshi et al. (1987). Thus, we have chosen the latter work as the base of our absorption intensity scale. It was not possible to correct the possible variations of the spectral response of this study because of the very poor accuracy of available TP data for highly excited and autoionizing levels involved in it. However, the scale of intensities of Joshi et al. (1987) were found to be roughly flat across their wavelength range (below 1207 Å) and similar in magnitude to intensities observed in emission by Kaufman (1982). Thus, for intensities observed in absorption, we give in Table 3 the values originally reported by Joshi et al. (1987) multiplied by 100 to roughly match the scale of emission intensities. Intensity values reported by Sarma & Joshi (1984) are smaller than those of Joshi et al. (1987) by a factor of 14 on average. Ratios of intensities observed in these two works vary within a factor of two on average with no discernible systematic trend as a function of wavelength. Thus, intensities of the two lines of Sarma & Joshi (1984) absent in Joshi et al. (1987) were reduced to the scale adopted in Table 3 by using ratios of observed intensities of several closely lying lines.

3.6. The State of Analysis of S I

Despite the great improvement in the accuracy of the presently reported S I spectral data, one should be cautioned about multiple existing problems. The most important is the existence of many tens of observed lines that cannot be identified with the presently known energy levels. Such unidentified lines are present in the line lists of Meißner et al. (1933), Frerichs (1933), Joshi et al. (1987), and Gibson et al. (1986). We have also observed a few tens of unidentified IR lines that are likely due to S I, but we do not give their list because many or all of them can be due to other constituents of our discharge plasma (He I, O I, N I, Ar I) and their relative observed intensities are difficult to reduce to a sensible unified scale.

The second problem is the absence of a complete dependable theoretical interpretation of this spectrum. The observed S I spectrum is difficult to interpret because of strong interactions between Rydberg series built on different terms of the ionic core. For this reason, even configurations with low principal quantum numbers, e.g., $3p^3(^2D^o)3d$, are not fully known. Martin et al. (1990) made great progress in reconciling conflicting interpretations of many autoionizing series observed

in absorption Joshi et al. (1987), Gibson et al. (1986), Sarma & Joshi (1984), and Tondello (1972). However, this left many observed absorption features uninterpreted. It is appropriate to quote their assessment here: “none of the available calculations is sufficiently accurate to allow definitive interpretation of all features of this complex spectrum” (Martin et al. 1990). More than 30 years later, this statement still remains true.

The calculation of Kurucz (2004) represents the latest progress in the analysis. At first glance, it seems to provide a comprehensive description for the most significant part of the spectrum. This was a parametric least-squares fit (LSF) with Kurucz’s own version of Cowan’s codes Cowan (1981). He included 61 even configurations, $3s^23p^4 + 3s^23p^3[np(n=4 \text{ to } 16) + nf(n=4 \text{ to } 17) + nh(n=6 \text{ to } 9) + nk(n=8, 9)] + 3s3p^4[ns(n=4 \text{ to } 16) + nd(n=3 \text{ to } 16)]$, and 61 odd configurations, $3s^23p^3[ns(n=4 \text{ to } 16) + nd(n=3 \text{ to } 16) + ng(n=5 \text{ to } 9) + ni(n=7, 8, 9)] + 3s3p^5 + 3s3p^4[np(n=4 \text{ to } 15) + nf(n=4 \text{ to } 16)]$. Kurucz had used all information about experimentally known energy levels provided by Martin et al. (1990) and Kaufman & Martin (1993) with some additions from his own interpretation of these data. This included 340 even and 281 odd experimental levels (a much larger set in comparison to 114 even and 263 odd levels established in the present work; however, most of Kurucz’s extension is due to his splitting of the quasi-degenerate configurations observed by Pratt (1988) into fine-structure levels). Of these levels, 7 even and 24 odd ones were excluded from the LSF. The experimental levels were fitted with 26 free parameters in the even parity and 48 in the odd parity. The standard deviations reported by Kurucz’s code in his log files are 7.5 cm^{-1} and 35 cm^{-1} , respectively. However, a few of the experimental even-parity levels were assigned to wrong theoretical eigenvectors. Namely, the experimental $3p^3(^4S^o)8p \ ^3P_{1,2}$ levels at $80,995.6 \text{ cm}^{-1}$ and $80,996.03 \text{ cm}^{-1}$ (Martin et al. 1990) were assigned to the theoretical $3p^3(^4S^o) \ ^5P_{1,2}$ levels; the experimental $3p^3(^4S^o)7p \ ^3P_2$, $3p^3(^4S^o)6f \ ^3F_2$, and $3p^3(^4S^o)6f \ ^3F_2$ levels at $80,112.93 \text{ cm}^{-1}$, $80,494.31 \text{ cm}^{-1}$, and $80,495.24 \text{ cm}^{-1}$ (Martin et al. 1990) were assigned to the theoretical $3p^3(^4S^o)6f \ ^3F_2$, $3p^3(^4S^o)7p \ ^3P_2$, and $3p^3(^4S^o)6f \ ^5F_2$ levels, respectively; and the experimental $3p^3(^2D^o_{3/2})7f$ level at $96,160 \text{ cm}^{-1}$ with $J=2$ (identified by Pratt 1988) was assigned to the theoretical $3p^3(^2D^o)8p \ ^1D_2$ level. We have corrected these assignments in Kurucz’s transition data file while evaluating his TP data (see Section 3.4) and reducing the observed intensities (see Section 3.5). Similar mistakes in level assignments were made for a few odd-parity levels above $94,000 \text{ cm}^{-1}$. After correction of the corresponding residuals of Kurucz’s LSF and inclusion of the omitted levels, the recalculated standard deviations of his LSF are 46 cm^{-1} and 205 cm^{-1} in the even and odd parity, respectively. This is still an impressively good accuracy. Only a few of the calculated even levels deviate from the experimental ones by more than 45 cm^{-1} , the largest deviation being 360 cm^{-1} . In the odd parity, the quality of the LSF is significantly worse, but still 90 % of calculated levels are within 100 cm^{-1} from the experimental ones. The largest deviations, up to 1100 cm^{-1} , are seen for highly excited levels of the $3p^3(^2D^o)3d$, $3p^3(^2P^o)3d$, and $3p^3(^2P^o)4d$ configurations. These large deviations appear to be due to strong interactions of these configurations with each other, as well as with several other configurations. These interactions are hard to describe in the frame of the LSF. They have a dramatic effect on the calculated TPs, which as a consequence have very poor accuracy for the affected levels.

The overall good quality of Kurucz’s LSF makes it possible to state that it is highly probable that the assignments of several

experimental odd-parity levels to the $^3P^o$ and $^3D^o$ terms of the $3p^3(^2P^o)nd$ configurations with $n \geq 5$ (deduced by Martin et al. 1990) from absorption spectroscopy studies) need to be interchanged. We have left them unchanged because it should be done in a more comprehensive study dedicated to interpretation of absorption spectra.

It should be noted that a comparable accuracy of calculated energy levels was achieved in the ab initio calculation of Zatsarinny & Bartschat (2006). For the 97 levels listed in their Table 1, the average deviation of theory from experiment is only 80 cm^{-1} . However, this paper lacks a detailed description of level composition and of the method used to identify theoretical levels with experimental ones. Their listed energy levels generally do not agree with the wavelengths listed in their supplementary data file. That file contains transitions involving many more levels than listed in their Table 1, but we did not find it possible to derive their calculated energies from the given wavelengths due to the inconsistencies mentioned above. Thus, a complete comparison of energy levels calculated by Zatsarinny & Bartschat (2006) with experiment is not possible. We also noticed that all A_{ki} values in that supplementary data file are incorrect because they are incompatible with the listed f_{ik} , S , and wavelength values. However, the f_{ik} and S values agree well with each other, which makes us confident that they are correct, while the errors in the A_{ki} values are due to a technical mistake. We have used their S values in combination with experimental wavelengths to derive the $g_k A_{ki}$ values given in Table 3 with a reference to Zatsarinny & Bartschat (2006).

4. Concluding Remarks

Accurate atomic spectroscopic data (e.g., wavelengths and energy levels) are crucial for interpretation of the growing amount of astrophysical data recorded by the ground and space observatories. Reliable and accurate spectroscopic data can be obtained from high-precision laboratory measurements. Astrophysical observations can also be an important, and sometimes the only, source of reliable atomic data, e.g., for weak transitions from metastable levels that cannot be seen in laboratory. However, improvement of quality of laboratory data is of the highest priority.

In this work, by using IR FT spectroscopy with a Bruker IFS 120 spectrometer, we have performed high-precision measurements of neutral atomic sulfur (S I) spectra in a wide IR domain including the wavelengths longer than $5 \mu\text{m}$, which have not previously been observed in laboratory experiments. We have described our methodology of using an IR FTS in acquiring accurate data. Our measurements, combined with previously published line lists, extend and improve the available S I data on wavelengths and energy levels of atomic sulfur. As a result of this work, uncertainties in all 179 presently known S I energy levels below ionization limit have been reduced by a factor of five on average. Our level list includes 114 even and 263 odd levels. Out of these, six levels have been observed and determined for the first time. They correspond to the $3p^3(^4S^o)ng$ ($n=5, 6, 7$), $3p^3(^4S^o)nh$ ($n=6, 7$), and $3p^3(^4S^o)7i$ quasi-degenerate configurations. In addition, three previously known levels have been revised. The present line list includes 869 transitions corresponding to 664 unique observed lines. Out of these, 191 transitions corresponding to 152 distinct lines were observed in our IR spectra for the first time. We have also extended the set of critically evaluated data on S I transition

probabilities by evaluating the accuracy of TPs calculated by Zatsarinny & Bartschat (2006) and Kurucz (2004). We have added 141 TP values from these two works to the set of TPs critically evaluated by Podobedova et al. (2009). In addition, we have improved the description of the S I spectrum by reducing all line intensities observed in laboratory emission experiments to a common uniform scale.

It should be noted that some important aspects of the S I spectrum (e.g., a comprehensive revision of critically evaluated transition probabilities and revision of the analysis of absorption spectra) are outside the scope of the present work. In addition, we have many (about 50) unidentified lines in our spectra, which do not necessarily belong to the S I spectrum since our discharge experiment was done in helium atmosphere (possibly contaminated by oxygen and/or nitrogen). Note that there are at least several tens of unidentified lines listed in previous publications by Meißner et al. (1933), Frerichs (1933), Jakobsson (1967), Joshi et al. (1987), and Gibson et al. (1986).

From the newly measured nonpenetrating (high- l) Rydberg levels, we have derived an improved value of the first ionization energy of the S atom, $IE = 83,559.170(11) \text{ cm}^{-1}$. This agrees with the previously recommended value, $83,559.1(10) \text{ cm}^{-1}$ (Martin et al. 1990), but the uncertainty has been reduced by 2 orders of magnitude.

Acknowledgments

A.K. acknowledges that the present work was conducted in the framework of a long-standing collaboration between NIST and J. Heyrovský Institute of Physical Chemistry (Academy of Sciences of the Czech Republic), which was established in 2019 for analysis of atomic spectra.

We are grateful to Dr. Emmanuil G. Silkis of the Institute of Spectroscopy, Troitsk, Russia for informing us about the error in the wavelength of the line listed as 10633.080 \AA in the NIST ASD.

P.K. acknowledges the support from the Czech Science Foundation (grant No. 20-10591J) and the Advanced Multi-scale Materials for Key Enabling Technologies project, supported by the Ministry of Education, Youth, and Sports of the Czech Republic. Project No. CZ.02.01.01/00/22_008/0004558, cofunded by the European Union.

V.Ch. acknowledges the support from the Russian Science Foundation (grant number 24-22-00238, <https://rscf.ru/en/project/24-22-00238/>).

ORCID iDs

S. Civiš  <https://orcid.org/0000-0001-6215-0256>
 A. Kramida  <https://orcid.org/0000-0002-0788-8087>
 E. M. Zanozina  <https://orcid.org/0000-0002-4890-6376>
 J. Kubišta  <https://orcid.org/0000-0002-5746-9315>
 P. Kubelík  <https://orcid.org/0000-0002-8498-6668>
 M. Ferus  <https://orcid.org/0000-0003-4008-2920>
 V. E. Chernov  <https://orcid.org/0000-0003-4027-4981>

References

- Alder, J. F., Bombelka, R. M., & Kirkbright, G. F. 1978, *JPhB*, **11**, 235
 Anderson, D. E., Bergin, E. A., Maret, S., & Wakelam, V. 2013, *ApJ*, **779**, 141
 Aufmuth, P., Heilig, K., & Steudel, A. 1987, *ADNDT*, **37**, 455
 Ballester, G. E., Moos, H. W., Feldman, P. D., et al. 1987, *ApJ*, **319**, L33
 Beideck, D., Schectman, R., Federman, S., & Ellis, D. 1994, *ApJ*, **428**, 393
 Bernard-Salas, J., Pottasch, S. R., Gutenkunst, S., Morris, P. W., & Houck, J. R. 2008, *ApJ*, **672**, 274
 Berzins, U., Luo, C., Zerne, R., Svanberg, S., & Biémont, E. 1997, *PhRvA*, **55**, 1836
 Biémont, E., Garnir, H., Federman, S., Li, Z., & Svanberg, S. 1998, *ApJ*, **502**, 1010
 Biémont, E., Storey, P., & Zeippen, C. J. 1996, *A&A*, **309**, 991
 Brault, J. W. 1987, *AcMik*, **93**, 215
 Bridges, J., & Wiese, W. 1967, *PhRv*, **159**, 31
 Brown, J. M., Evenson, K. M., & Zink, L. R. 1994, *ApJL*, **431**, L147
 Carpenter, K. G., Robinson, R. D., Wahlgren, G. M., Linsky, J. L., & Brown, A. 1994, *ApJ*, **428**, 329
 Chernov, V., Manakov, N., & Starace, A. 2000, *EPJD*, **8**, 347
 Civiš, S., Ferus, M., Chernov, V. E., & Zanozina, E. M. 2013, *A&A*, **554**, A24
 Civiš, S., Ferus, M., Kubelík, P., Chernov, V. E., & Zanozina, E. M. 2012a, *A&A*, **545**, A61
 Civiš, S., Ferus, M., Kubelík, P., Jelínek, P., & Chernov, V. E. 2012b, *A&A*, **541**, A125
 Civiš, S., Ferus, M., Kubelík, P., et al. 2012c, *A&A*, **542**, A35
 Civiš, S., Kubelík, P., Ferus, M., et al. 2018, *ApJS*, **239**, 11
 Civiš, S., Szabla, R., Szyja, B. M., et al. 2016, *NatSR*, **6**, 23199
 Cowan, R. D. 1981, *The Theory of Atomic Structure and Spectra* (Berkeley, CA: Univ. of California Press)
 Doering, J. 1990, *JGR*, **95**, 21313
 Durrance, S. T., Feldman, P. D., & Weaver, H. A. 1983, *ApJL*, **267**, L125
 Edlén, B. 1964, in *Handbuch der Physik, Spektroskopie I*, ed. S. Flügge, Vol. 5 (Berlin: Springer Verlag), 8
 Eriksson, K. 1978, *ApJ*, **222**, 398
 Feaga, L. M., McGrath, M. A., & Feldman, P. D. 2002, *ApJ*, **570**, 439
 Federman, S. R., & Cardelli, J. A. 1995, *ApJ*, **452**, 269
 Frerichs, R. 1933, *ZPhy*, **80**, 150
 Froese Fischer, C., Tachiev, G., & Irimia, A. 2006, *ADNDT*, **92**, 607
 Gibson, S. T., Greene, J. P., Rušćić, B., & Berkowitz, J. 1986, *JPhB*, **19**, 2825
 Gordon, I., Rothman, L., Hargreaves, R., et al. 2022, *JQSRT*, **277**, 107949
 Haas, M. R., Hollenbach, D., & Erickson, E. F. 1991, *ApJ*, **374**, 555
 Hase, F., Wallace, L., McLeod, S. D., Harrison, J. J., & Bernath, P. F. 2010, *JQSRT*, **111**, 521
 Heckert, N., Filliben, J., Croarkin, C., et al. 2012, *NIST/SEMATECH e-Handbook of Statistical Methods* (Gaithersburg, MD: National Institute of Standards and Technology)
 Hibbert, A. 1980, *JPhB*, **13**, 3725
 Jakobsson, L. 1967, *Ark. Fys.* (Stockholm), **34**, 19
 Joshi, Y. N., Mazzoni, M., Nencioni, A., Parkinson, W. H., & Cantu, A. 1987, *JPhB*, **20**, 1203
 Kama, M., Shorttle, O., Jermyn, A. S., et al. 2019, *ApJ*, **885**, 114
 Kaufman, V. 1982, *PhysS*, **26**, 439
 Kaufman, V., & Martin, W. 1993, *JPCRD*, **22**, 279
 Keller, J. C. 1973, *JPhB*, **6**, 1771
 Kramida, A. 2013, *FuST*, **63**, 313
 Kramida, A. 2021, A suite of atomic structure codes originally developed by R. D. Cowan adapted for Windows-based personal computers, NIST Public Data Repository, doi:[10.18434/T4/1502500](https://doi.org/10.18434/T4/1502500)
 Kramida, A., Ralchenko, Y., Reader, J., & NIST ASD Team 2023, *NIST Atomic Spectra Database, v5.11* (Gaithersburg, MD: National Institute of Standards and Technology), <https://physics.nist.gov/asd>
 Kramida, A., Ryabtsev, A. N., & Young, P. R. 2022, *ApJS*, **258**, 37
 Kramida, A. E. 2011, *CoPhC*, **182**, 419
 Kubelík, P., Civiš, S., Pastorek, A., et al. 2015, *A&A*, **582**, A12
 Kurucz, R. L. 2004, *Calculations for S I in the Atoms Collection* (Cambridge, MA: Harvard-Smithsonian Center for Astrophysics), <http://kurucz.harvard.edu/atoms.html>
 Kwitter, K. B., & Henry, R. B. C. 2001, *ApJ*, **562**, 804
 Lai, K.-F., Salumbides, E. J., & Ubachs, W. 2020, *JPhB*, **53**, 175002
 Martin, W. C., Zalubas, R., & Musgrove, A. 1990, *JPCRD*, **19**, 821
 Meija, J., Coplen, T., Berglund, M., et al. 2016, *PApCh*, **88**, 293
 Meißner, K. W., Bartelt, O., & Eckstein, L. 1933, *ZPhy*, **86**, 54
 Milingo, J. B., Kwitter, K. B., Henry, R. B. C., & Cohen, R. E. 2002, *ApJS*, **138**, 279
 Müller, D. 1968, *ZNatA*, **23**, 1707
 OPUS 2004, *OPUS Spectroscopic Software, Reference Manual v5*, <http://www.bruckeroptics.com/opus.html>
 Papoušek, D., Ogilvie, J., Civiš, S., & Winniewisser, M. 1991, *JMoSp*, **149**, 109
 Peck, E. R., & Reeder, K. 1972, *JOSA*, **62**, 958
 Podobedova, L. I., Kelleher, D. E., & Wiese, W. L. 2009, *JPCRD*, **38**, 171
 Pratt, S. T. 1988, *PhRvA*, **38**, 1270
 Ryde, N., Hartman, H., Oliva, E., et al. 2019, *A&A*, **631**, L3

- Sarma, V., & Joshi, Y. 1984, *PhyBC*, 123, 349
- Seaton, M. J. 1983, *RPPh*, 46, 167
- Tondello, G. 1972, *ApJ*, 172, 771
- Turrini, D., Schisano, E., Fonte, S., et al. 2021, *ApJ*, 909, 40
- Veseth, L. 1985, *PhRvA*, 32, 1328
- Visscher, C., Lidders, K., & Bruce Fegley, J. 2006, *ApJ*, 648, 1181
- Walsh, C. 2020, *The Chemical Biology of Sulfur* (London: Royal Society of Chemistry)
- Wang, M., Huang, W. J., Kondev, F. G., Audi, G., & Naimi, S. 2021, *ChPhC*, 45, 030003
- Wiese, W., Smith, M., & Miles, B. 1969, *Atomic Transition Probabilities. Vol. 2: Sodium through Calcium: A Critical Data Compilation* (National Bureau of Standards: Washington, D.C), <https://nvlpubs.nist.gov/nistpubs/Legacy/NSRDS/nbsnsrds22.pdf>
- Zatsarinny, O., & Bartschat, K. 2006, *JPhB*, 39, 2861
- Zerne, R., Caiyan, L., Berzinsh, U., & Svanberg, S. 1997, *PhyS*, 56, 459